8-2024

Quantifying Plot-Scale Evapotranspiration in Northeast Utah

W. Sheridan Stewart
Utah State University

QUANTIFYING PLOT-SCALE EVAPOTRANSPIRATION IN NORTHEAST UTAH

by

W. Sheridan Stewart

A thesis submitted in partial fulfillment
of the requirements for the degree

of

MASTER OF SCIENCE

In

Civil and Environmental Engineering

Approved:

_____	_____
J. Burdette Barker, Ph.D., P.E. Major Professor	Lawrence Hipps, Ph.D. Committee Member
_____	_____
Alfonso Torres-Rua, Ph.D. Committee Member	D. Richard Cutler, Ph.D. Vice Provost of Graduate Studies

UTAH STATE UNIVERSITY
Logan, Utah

2024

ABSTRACT

QUANTIFYING PLOT-SCALE EVAPOTRANSPIRATION IN NORTHEAST UTAH

by

W. Sheridan Stewart, Master of Science

Utah State University, 2024

Major Professor: Dr. J. Burdette Barker
Department: Civil and Environmental Engineering

The aim of this study was to quantify evapotranspiration on a plot scale in Northeastern Utah. The plot scale is often used for crop and irrigation management. In this study, ground-based canopy sensing stations and the Two-Source Energy Balance were used to model to quantify evapotranspiration in an alfalfa-grass mix hay field under a wheel-line irrigation system. The plot chosen was adjacent to an eddy covariance tower, against which the modeled data were validated. Data collection occurred in the growing seasons of 2022 and 2023. Two sensing stations were assembled and maintained for both years. Station 1 remained stationary during the study. Station 2 remained stationary for 2022 and was moved throughout the field in 2023. Both stations included infrared radiometric thermometers for land surface temperature, red and near-infrared radiometers, and canopy photography. Station 1 also included sensor instrumentation for measuring air temperature, relative humidity, barometric pressure, and wind speed, gust, and direction. Leaf area index measurements were collected throughout 2023. Crop height was measured every time a researcher was at the site. The eddy covariance tower

provided incoming solar radiation. These data were sufficient to run the Two-Source Energy Balance model. The Two-Source Energy Balance model requires inputs of canopy biophysical properties. A code was developed to find fraction of vegetative cover from canopy photography. This method was validated against existing relationships documented between the Normalized Difference Vegetation Index and fraction of vegetative cover. Leaf area index was modeled using a relationship with fraction of vegetative cover and was validated against observed measurements taken in 2023. Crop height was modeled from a relationship with the Soil Adjusted Vegetation Index and validated against observed measurements. All four energy balance fluxes were compared against the eddy covariance fluxes. Estimated evapotranspiration was evaluated against the eddy covariance tower evapotranspiration. Several different data inputs into the model were investigated, including different timesteps, modeled vs. eddy covariance calculated soil heat flux, and time of day. The results of the study were mixed. Station implementation and modeling efforts were accomplished on a continuous plot scale. Evapotranspiration was biased high. Evapotranspiration responded to seasonal patterns seen in the eddy covariance tower evapotranspiration. The eddy covariance tower does not force energy balance closure whereas the Two-Source Energy Balance model does. This may explain some bias.

(81 Pages)

PUBLIC ABSTRACT

Quantifying Plot-scale Evapotranspiration in Northeast Utah

W. Sheridan Stewart

Evapotranspiration, the combined movement of water from the earth's surface and plants to the atmosphere, is a component of the energy balance of the land surface atmosphere continuum. Often, irrigation is used to replace water removed from the soil through evapotranspiration. Water management for irrigation is often done at the plot or field scale. Due to the smaller footprint size and the large upfront costs, evaluating evapotranspiration at such a small scale can be difficult to justify. The aim of the study was to quantify evapotranspiration at the plot scale. An energy balance model that evaluates energy from two sources, the soil surface and the vegetation surface, was used to model the energy balance in an alfalfa-grass mix field in Northeastern Utah. Two canopy sensor stations used to collect data for this model were deployed throughout the growing seasons of 2022 and 2023. The stations were in proximity to an eddy covariance tower. The eddy covariance method is widely regarded as one of the best ways to sense actual, not modeled, evapotranspiration. The canopy sensing stations' energy fluxes were compared against the eddy covariance tower. During 2022, canopy Stations 1 and 2 were stationary. During 2023, Station 1 remained stationary, while Station 2 was moved around throughout the season. Some properties of the vegetation canopy were needed for the two-source model. Those primarily include fraction of vegetative cover, leaf area index, and crop height. These represent the percentage of viewing area that is covered by vegetation, the ratio of plant leaf area to ground area, and the height from the soil surface

of the crop. These vi properties were modeled with success from various methods. The model produced estimates of all four components of the energy balance, net radiation, sensible heat flux, soil heat flux, and latent heat flux (which is energy used in evapotranspiration). These components were then compared against the eddy covariance tower components. Latent heat fluxes were converted into evapotranspiration rates. Results were mixed. Stations were operated and continuously collected plot-scale data. Station evapotranspiration responded well to seasonal changes. However, station evapotranspiration was biased high through the entire growing season.

ACKNOWLEDGMENTS

My time at USU has been an adventure. I am very grateful to have had this opportunity. Guidance and friendship from Dr. Burdette Barker have been a worthwhile experience. Dr. Alfonso Torres-Rua and Dr. Larry Hipps have provided help and valuable insight into my work. A special thanks goes to Martin Schroader for his willingness to help with data and fieldwork. I want to thank my friends and brother, who all helped me understand the coding aspect of this research. Thank you to my family for helping to keep me grounded and, at times, sane. I want to acknowledge my friends who helped me maintain a social life, particularly Saneej, Moises, Nick M., Nick G., Jacob, and Owen. Finally, I would like to thank my wife, Holly, for the constant encouragement and for putting up with the many hours of weekend research.

- Sheridan Stewart

CONTENTS

Page

ABSTRACT iii

PUBLIC ABSTRACT v

ACKNOWLEDGMENTS vii

LIST OF TABLES x

LIST OF FIGURES xi

CHAPTER 1. INTRODUCTION 1

Research Objectives 2

CHAPTER 2. REVIEW OF RELATED LITERATURE 3

Water Balance 3
Lysimeters 3
Eddy Covariance Towers 4
Surface Remote Sensing for Evapotranspiration 4

Satellites 4
Unmanned Aireal Vehicles (UAVs) 6
Ground-Based Remote Sensing Equipment 6
Models 7

CHAPTER 3. MATERIALS AND METHODS 11

PyTSEB 11
Research Site and Weather Data Collection 11
Bio-Physical Properties 17

Fraction of Vegetative Cover 17

Leaf Area Index 19
Crop Height 19

Site Specific Inputs 20
Stations One and Two TSEB 21
Landsat 22

CHAPTER 4. RESULTS AND DISCUSSIONS 23

Bio-Physical Properties Results 23

Fraction of Cover 23
Leaf Area Index 26
Crop Height 29

PyTSEB 31

Unprotected 31
Protected 45

Chapter 5. CONCLUSIONS 53

Research Objective Tasks 53

Data Collection 53
Biophysical properties 53
TSEB and ET 54

Research Objective 54
Future Applications and Recommendations 55

References 56

Appendix 64

LIST OF TABLES

Page

Table 1 *Station Sensor Instrumentation* 12

Table 2 *Station 2, 2023 Location Time Periods.* 15

Table 3 *Site Specific PyTSEB Values* 21

Table 4 *2022 Calibration FoC Statistical Biases and Fit* 23

Table 5 *LAI Biases and Fit* 28

Table 6 *Crop Height Biases and Fit* 30

Table 7 *Calibration Data Biases and Fit* 31

Table 8 *Solar Noon Calibration Data Biases and Fits* 36

Table 9 Landsat biases and fit to eddy covariance tower 39

Table 10 Daily ET Values Biases and Fit 42

Table 11 2023 Data Biases and Fit 45

Table 12 Validation daily ET biases and fit. 50

LIST OF FIGURES

Page

Figure 1 *Utah State University Uintah Basin - Vernal Campus Research Field Right*... 13

Figure 2 *Station 1 2023 Canopy and Weather Instrumentation During Set Up* 14

Figure 3 *Research Field Features Approximate Locations*..... 16

Figure 4 *2022 FoC Calibration Comparison*..... 24

Figure 5 *2023 FoC Validation Comparison*..... 25

Figure 6 *Station 1 LAI Equation Development* 27

Figure 7 *Leaf Area Index Validation Comparison* 28

Figure 8 *Crop Height Equation Development*..... 29

Figure 9 *Crop Height Validation Comparison* 30

Figure 10 *2022 Modeled and Measured RN* 32

Figure 11 *2022 Modeled and Measured G*..... 33

Figure 12 *2022 Modeled and Measured H*..... 34

Figure 13 *2022 modeled and measured LE*..... 35

Figure 14 *Station 1 and 2 2022 Solar Noon Calibration Energy Summary* 37

Figure 15 *Modeled Calibration Dataset Energy Fluxes for Landsat, Stations 1 and Station 2* 40

Figure 16 *2022 Station 1 ET Timeseries* 43

Figure 17 *2022 Station 2 ET Timeseries* 43

Figure 18 *2022 Modeled and Measured ET*..... 44

Figure 19 *2023 Modeled and Measured RN* 46

Figure 20 *2023 Modeled and Measured H* 47

Figure 21 *2023 Modeled and Measured G* 48

Figure 22 *2023 Modeled and Measured LE* 49

Figure 23 *2023 Station 1 and Eddy Covariance ET Timeseries* 51

Figure 24 *2023 Station 2 and Eddy Covariance ET Timeseries* 51

Figure 25 *2023 Modeled and Measured ET* 52

Figure 26 *Station 1 2022 FoC Timeseries* 65

Figure 27 *Station 2 2022 FoC Timeseries* 65

Figure 28 *Station 1 2023 FoC Timeseries* 66

Figure 29 *Station 2 2023 FoC Timeseries* 67

Figure 30 *Hourly daytime RSO and Incoming Shortwave* 67

Fig. 31. Hourly daytime RSO and incoming shortwave. 67

Figure 32 *Hourly LE Fluxes with Eddy Covariance G* 68

Figure 33 *2022 Air Temperature Unity* 68

Fig. 34. 2022 air temperature unity. 68

Figure 35 *2022 Vapor Pressure Unity* 69

CHAPTER 1. INTRODUCTION

Water conservation in the Western United States has been a longstanding concern. The region's rapid population growth, coupled with the challenges posed by climate issues, has significantly heightened the urgency of addressing water availability across diverse use sectors. As water resource allocation continues to be a subject of investigation, particular attention is being directed towards reducing agricultural irrigation water use. In many areas, the need to reduce consumptive water use, including crop evapotranspiration (ET), is of primary interest.

The quantification of crop ET holds advantages for both research and management within the realm of irrigation practices. Aligning irrigation with the actual water consumed through ET is a common approach for ensuring efficient water use. Consequently, quantifying crop ET is important in furnishing information and aiding irrigation management decisions.

Concentrated efforts have been made to quantify ET with the intent of water optimization. Quantification efforts have generally focused on the basin or sub-basin scale or specific crop types. While this information is advantageous, farmers' and growers' irrigation management decisions are often made at field or plot-scales. Thus, quantifying ET specifically at a plot-scale is of interest for management and research purposes.

Quantifying ET directly (measuring) has a specific set of issues. Direct ET measurements involve knowledge and equipment, such as eddy covariance and weighing lysimeters, that can be difficult and expensive to obtain. When scaling down to the plot

scale, costs can become more difficult to justify. For these reasons, often quantification 2 efforts can take a less direct approach and estimate ET from a modeling process. Some ET models are discussed further in the literature review section.

One such model is the Two-Source Energy Balance (TSEB) model (Norman, 1995). This model has been used over a wide variety of applications. The advantage of the TSEB model is how it calculates the energy balance. It partitions the surface into representative soil and crop portions when modeling the energy balance. Modeled crop latent heat flux can be used to calculate daily ET.

Modeling efforts have allowed for furthering research on plot-scale ET. These efforts have usually been based on aerial or satellite imagery. Collecting data for models poses its own set of challenges. The temporal scale of aerial and satellite platforms is chief among those. Continuous monitoring is desirable for both research and management decisions. Aerial imagery is constrained by fly times, which can be done frequently but not continuously. Satellite imagery is constrained by satellite flyover (orbit) time. One technology platform that has shown promise for ET continuous modeling, is ground based remote sensing. Ground-based remote sensing platforms allow for the continuous monitoring of ET at the plot-scale. This provides insight into real-time ET requirements of the observed crop of the surface.

Research Objectives

The aim of this research was to accurately model plot-scale ET using TSEB with continuous ground-based remote sensing.

CHAPTER 2. REVIEW OF RELATED LITERATURE

A significant body of work exists for different methods of determining ET. This literature is discussed in the proceeding sections. Emphasis has been placed on those methods that are appropriate for determining plot-scale ET.

Water Balance

The water balance method is a common way of estimating ET primarily for irrigation management purposes (Simić, 2023). The method relies on the conservation of mass. The water outputs (ET, runoff, and deep percolation) must equal the water inputs (precipitation, irrigation, and run-on) plus the change in storage within the system's boundary volume. ET is found in the differences between the changes in storage and the other terms. Some components that pose a challenge in water balance calculations are discussed further. Common challenges with the water balance methods include quantifying runoff, subsurface lateral flow, deep percolation, and capillary rise (Bosch, 2005; Colaizzi, 2012b; Colaizzi, 2014; Katimbo, 2022a, b; Tunica, 2023; Marek, 2023; Laing, 2018; Trout, 2018; Mohammed; 2022; Hunsaker, 2005; Simić, 2023).

Lysimeters

Weighing lysimeters are an instrument that find ET by measuring changes in the weight of a control volume. Weight losses can be related to ET (Collaizi, 2014). This can be a desirable way of measuring evapotranspiration for multiple irrigation treatments (Sun, 2012). Microlysimeters can be used to find ET at the plot or field scale. This can find plot-scale ET directly or indirectly. Each plot or a set number of plots can have its own microlysimeter (Song, 2016). Due to the high cost of lysimeter installation and 4

maintenance, one large lysimeter can take the place of many microlysimeters in plot-scale research. A lysimeter can be placed at the end of the end of the plot areas if runoff and subsurface flow are desired to be found (Duncan, 2017). This can be advantageous for plot-scale research when using water balance methods.

Eddy Covariance Towers

An eddy covariance tower measures the vertical turbulent fluxes of momentum, heat, water vapor, and gases between the surface and the atmosphere. Eddy covariance towers are one of the most established methods of measuring ET (Denager, 2020). It can often be thought that eddy covariance towers underestimate ET, because the energy balance is not forced closed. Studies have shown that over longer periods (multiple years) eddy covariance latent heat fluxes can be similar to that of the water balance (Denager, 2020).

Surface Remote Sensing for Evapotranspiration

Surface Remote Sensing for Evapotranspiration

Surface remote sensing of ET generally involves measuring emitted and reflected long-wave irradiance and reflected short-wave irradiance. There are a variety of methods to measure these irradiances. Common methods for remotely sensing irradiances and common methods of estimating ET from those are discussed further, with emphasis placed on their adaptability to plot-scale research.

Satellites

One technology that has gained popularity within the last several decades is satellite remote sensing. Satellite remote sensing has several desirable advantages. Fast

data processing time is a key advantage, another is automation and labor intensity 5 (Steven, 1993).

When research is conducted on a small scale (e.g., plot), spatial resolution of many satellite products can be an issue. The most recent Landsat satellite has spatial resolutions of 15, 30, and 100 m, depending on the spectral band (Montanaro, 2022). Often times plot-scale research is smaller than 10-meters. To address this issue, downscaling satellite data and upscaling data collected from a source with a smaller footprint size to validate data against satellite data has been investigated with positive success (Anderson, 2004). Other attempts to investigate this issue have used satellite image sharpening, sharpening an image with a larger pixel size and finer spectral or temporal resolution with an image with a smaller pixel size coarser spectral or temporal resolution. This has shown some positive results but has so far underestimated transpiration (Bellvert, 2020).Another issue when evaluating satellite-collected data for plot-scale research can be the timing. Satellite data is bound by the Satellite's fly-over (orbit) time. When critical time points or continuous monitoring are desired to be investigated, the researchers are subject to the timing of the satellite orbit. Research into temporal resolution scaling has been investigated using hybrid gap-filling methods and pulling data from multiple satellite sources. This has demonstrated low bias. (Bellvert, 2020; Guzinski, 2023).

Another issue when evaluating satellite-collected data for plot-scale research can be the timing. Satellite data is bound by the Satellite's fly-over (orbit) time. When critical time points or continuous monitoring are desired to be investigated, the researchers are subject to the timing of the satellite orbit. Research into temporal resolution scaling has

been investigated using hybrid gap-filling methods and pulling data from multiple satellite sources. This has demonstrated low bias. (Bellvert, 2020; Guzinski, 2023).

It is noteworthy that some satellites have more frequent flyover times and very high spatial resolutions. However, as of this writing, the data from those satellites have a fee to access and use.

Unmanned Aireal Vehicles (UAVs)

Another common data collection method is the use of unmanned aerial vehicles (UAVs or drones). As the availability of UAVs has risen, so has the customizability of the remote sensing instrumentation that can be mounted on a UAV platform (Neito, 2018). UAV remote sensing can provide data with a quick turnaround time (Berni, 2009). This is desirable when making irrigation management decisions. UAV sensing can be resourceful. Overlapping flight paths can help to ascertain accurate sensing, particularly for pixels on thermal images (Tunica, 2023). This can be helpful for plot-scale ET evaluation when plot areas are clearly defined.

Ground-Based Remote Sensing Equipment

Another data collection platform is ground-based remote sensing. Ground-based remote sensing can have many different approaches. Approaches can have a measurement footprint size of hundreds of square-meters down to less than 1 m2. This can have many advantages for plot-scale research. Another advantage of ground-based approaches is that continuous monitoring can be available. This is desirable when compared to satellites and UAV platforms that are bound by orbit and fly times. This is desirable for management purposes.

Real-time ET can be continuously estimated from ground-based platforms. For example, from canopy temperatures derived from infrared sensors (Katimbo, 2022a, b). Continuous monitoring and quick data turnaround time can be advantageous for making real-time management decisions (Colaizzi, 2012).

Models

Many models exist to find ET through remote sensing inputs. This is often done through the energy balance. The energy balance is the equation describing the energy exchange between the land surface-atmosphere continuum. It consists of net radiation (RN), soil heat flux (G), sensible heat flux (H), and latent heat flux (LE). Many involve modeling H, RN, and G. The LE (used to calculate ET) is then found from the residual. Some of the more common models used in that area appropriate for plot-scale research are discussed below.

SEBAL and METRIC

Surface Energy Balance Algorithms for Land (SEBAL) (Bastiaanssen, 1998) is a satellite-based image-processing model that calculates ET as a residual of a surface energy balance (Allen, 2011). SEBAL was developed with surfaces with a large hydrological contrast in mind (Bastiaanssen, 1998). Mapping ET at high resolution with internalized calibration (METRIC) is based on the SEBAL model (Allen, 2007). Both models focus on finding “hot” and “cold” pixels to anchor the calculation process. METRIC estimates ET based on the residual surface energy balance. The surface energy balance is calibrated internally against reference ET (Allen, 2007).

SEBAL and METRIC hold several advantages. Primarily, in both models, the near-surface temperature gradient is estimated as an indexed function of radiometric surface temperature. This eliminates the need for air temperature measurements and extremely accurate land surface temperatures (Singh, 2008).

The main data input for both models is land surface temperature (LST) images from satellite-collected data. Due to satellite spatial resolution limitations discussed 8 earlier, the pixel size resolution is limited to that of LST images. Therefore, the plot-scale size is limited by LST resolution size. This can make plot-scale research difficult using these models. However, scaling methods such as those discussed in the satellite section can be used for plot-scale research.

Reflectance-Based Crop-Coefficients

Reflectance-based crop coefficients have been used to estimate ET for decades. Crop coefficient models use a crop-specific coefficient (Kc) multiplied by a reference ET value to estimate crop ET (Trout, 2018). Different versions of crop coefficient models have been developed. One of the more prominent of those is the basal crop coefficient, which estimates transpiration through a non-stressed crop and slow diffusive evaporation through a dry soil surface (Bausch, 1987; Trout, 2018). Basal crop coefficient methods have been found to work best for early-stage plant growth for closed canopy crops (Trout, 2018).

Much of the research to date has used large plots on hundreds to thousands of m2 (Douglas, 2005; Bausch, 1994). These methods have shown promise for large-scale plots.

Multiple ET Quantification Models

Research has been conducted using multiple methods to quantify ET and ET uncertainty. This type of research often attempts to determine the accuracy and bias of existing ET estimation methods or inter- and intra-ET model comparisons. Kustas (2012) compares ET estimation methods within the same model. Researchers such as Laing (2021) and Katimbo (2022b) investigated ET estimation between two models. Barker (2018) investigated the hybridization of two models.

While some of these works and others do not focus on ET at the plot-scale, they 9 provide valuable insight into the results of ET estimation from multiple sources. Kustas (2012) looked at the unity between estimated ET using the TSEB model and a dual-time difference model. While the uncertainty is not calculated, agreement between the two models is found to be acceptable.

TSEB

The TSEB was developed in 1995 by Norman et. al. The model was one of the first to explore latent and sensible heat fluxes from two sources (soil and vegetation). The model uses a relationship between brightness, temperature gradient, and weather data to partition the energy balance components into soil and vegetation sources. Although at a single view angle, only composite temperature is available, partitioning temperature can be done through fraction of vegetative cover.

The TSEB model has been used in numerous applications. One important group of studies was done at the U.S. Department of Agriculture's Agriculture Research Service Conservation and Production Research Laboratory in Bushland, Texas. Several modifications of the TSEB model were evaluated there. This research included testing of

the TSEB model against lysimeter measured ET. This has been an uncommon occurrence (Colaizzi, 2016). The original TSEB model uses the Priestly-Taylor approximation to find the canopy temperature of the soil-vegetation surface. Some of the work in Bushland was included in evaluating the TSEB model using the Penman-Monteith approximation (Colaizzi, 2012b; Colaizzi, 2014). Other methods at Bushland consisted of nonspatial vegetation distribution was evaluated as elliptical hedgerows instead of the traditional semi-empirical clumping index for row crops with partial canopy covers (Colaizzi, 10 2012a).

The TSEB model is appropriate at any spatial scale and has been applied to many. Some of the inputs TSEB are more sensitive to include, leaf area index (LAI) and fraction of vegetative cover (FoC), which tend to be more homogenous for close-seeded crops on the plot-scale. Measurements and modeling of these inputs is of great importance for TSEB based research.

CHAPTER 3. MATERIALS AND METHODS

PyTSEB

This research used the PyTSEB code (Python-coded TSEB model, open-source code written by Neito et. al.) implementation of the TSEB model. PyTSEB requires several inputs. When using PyTSEB over a timeseries several inputs are required at each time step. The broad input categories required are local weather data and crop biophysical properties. These are discussed in their appropriate sections below. Several site-specific options also need to be specified. These are discussed in detail in its representative section.

Research Site and Weather Data Collection

To evaluate accuracy, a few sites near an eddy covariance tower were considered to conduct the research. Of the sites available, the most desirable for potential future applications beyond this project was on the Utah State University Uintah Basin – Vernal Campus's agriculture field in Vernal, Utah. This field was chosen to conduct the research. The site produced an alfalfa-grass mix hay crop. The crop is irrigated under a side roll (wheel-line) irrigation system. The research was conducted at this site throughout the growing seasons of 2022 and 2023.

Two canopy sensing stations were used throughout the research. In 2022 both stations were stationary. Both stations were located approximately 33 m to the east of the eddy covariance tower. Station 1 was located approximately 17 m to the South of Station 2. Both stations included canopy sensors. The proximal infrared temperature radiometer and the red-near infrared radiometers faced nadir. Station 1 included weather data sensors

12 as well. A summary of each station's sensors is described in Table 1. Sensor observations were sampled every 10 seconds with an average recorded every 15 minutes.

Table 1

Station Sensor Instrumentation

Sensor	Sensor Make and Model	Station(s)
Proximal infrared temperature radiometer	Apogee Instruments SI-411-SS	1 and 2
Red-near infrared radiometers	Apogee Instruments S2-411-SS and S2-412-SS	1 and 2
Relative humidity Probe	Apogee Instruments EE08-SS with Apogee Instruments TS-120-SS V Shield as the aspirated shielding	1
Barometric Pressure	Campbell Scientific CS106	1
Wind speed	Meter Group ATMOS 22	1

Further, incoming shortwave radiation is needed for the TSEB model input. Before research commenced an order for a net radiometer sensor was placed. The sensor was on back order for the duration of this research. Due to the backorder, this data were collected from the nearby eddy-covariance tower. Figure 1 and Figure 2 are images of the locations of the stations within the research field and the sensory setup of Station 1 respectively.

Figure 1

Utah State University Uintah Basin - Vernal Campus Research Field Right

Note: The left image is the entire field. The right image is the eddy covariance tower, station 1 2022, 2023; and station 2 2022 location. Image sourced from ESRI, 2011.

Figure 2

Station 1 2023 Canopy and Weather Instrumentation During Set Up

In 2022, data collection began on June 13th and ended on November 5th. In 2023, data collection began on April 29th and ended on November 9th. The 2023 setup of Station 1 was identical to the 2022 setup. To evaluate performance on different portions of the field, and to determine the viability of future deployment, Station 2 was moved to various locations throughout the testing period. The location time periods are listed in Table 2.

A few site constraints limited Station 2's mobility. To reduce labor for the grower, the station's location was limited in the East/ West directions by the joints in the irrigation

wheel-line system. Primarily, when the irrigation system moved past a station, the pipeline had to be taken apart at a joint and manually wheeled around the station equipment. This joint was about 62 m West of the system riser locations. A few other location constraints existed. These constraints are depicted in Figure 3.

Table 2

Station 2, 2023 Location Time Periods.

Location	Time Period
A	05/08/23 – 05/20/23
B	05/20/23 – 06/01/23
C	06/01/23 – 06/27/23
D	06/27/23 – 07/11/23
E	07/11/23 – 08/02/23
F	08/02/23 – 08/17/23
G	08/17/20 – 08/30/23
H	08/30/23 – 09/30/23
I	09/30/23 – 11/05/23

Note: Letters correspond with those in Figure 3.

Figure 3

Research Field Features Approximate Locations

Note: The vertical line represents the primary East/West Constraint. The diamond shapes represent the approximate riser locations, spaced 60 m apart. The letters represent the location of Station 2. Image sourced from ESRI, 2011.

The crop is a multiple harvest (cutting) per-season hay crop. The research field grower's equipment could not fit in some of the areas surrounding Stations 1 and 2, and the eddy covariance tower. To simulate cuttings for the areas under the measurement sensors, a researcher performed a manual cut within one week after the rest of the field was cut. The researchers cut the crop to the same length as the surrounding crop. The

crop was then gathered (raked) and placed into an adjacent windrow. Times while the researcher was within the footprint of the equipment were recorded, and the corresponding data were discarded.

Bio-Physical Properties

Fraction of Vegetative Cover

The fraction of vegetative cover (FoC) is a crop biophysical input in the TSEB model. FoC was estimated using two methods based on canopy photographs and shortwave reflectance measurements, respectively. Camera photography and a developed clustering code were used as the observed calibration data. Each station was equipped with a canopy RGB camera. Camera photographs were recorded every hour. Established relationships between a vegetation index, derived from incoming red and near-infrared reflectance values, and FoC served as the calibration data.

When developing the code for finding daily FoC from the camera RGB images, multiple methods were considered to determine. Existing software packages to cluster the canopy images into vegetation and non-vegetative pixels were evaluated. Arc-Pro GIS, Arc GIS, and Canopeo were among those.

Ultimately, code was written with the researchers' specifications. The code masked the RGB camera images to the same size and location as the proximal infrared radiometer footprint. The masked image was then clustered according to pixel color via a K-means clustering algorithm. The number of clusters was based on the within-cluster sum of square values plotted against the number of K clusters. The point of diminishing values gained by adding one cluster was identified and used as the number of clusters.

This is often referred to as the “elbow” method (Umargono, 2019). An upper limit of ten clusters was used.

After clustering, the user was prompted to decide to place each cluster into one of five groupings. The groups were “vegetation,” “non-vegetative,” “shaded vegetation,” 17 “shaded non-vegetative,” and “shadow.” The code saved the total pixel counts for each group to a CSV file. Some issues occurred with dew formation on the camera lenses. To combat this, desiccant packs were attached to each camera.

FoC was then calculated by dividing the number of vegetative pixels by the total number of pixels. It was ultimately decided to ignore shaded pixels as they were not representative of the surface the shadow was on. To limit shadow, solar noon images were selected for daily FoC. If solar noon had occurred within two hours of precipitation, or an irrigation event, had dew on the camera lens, or was unavailable due to camera malfunctions; images within two hours of solar noon were evaluated. Preference order was given for one hour before, then one hour after, then two hours before, and two hours after solar noon. If no image was available within two hours of solar noon, PyTSEB was not calculated during those days.

For comparison data, red and near-infrared reflectance values were calculated from the radiometers. The Normalized Difference Vegetation Index (NDVI) was calculated from the reflectance values. FoC was calculated from the relationship set forth by Choudhury et al. (1994) equation 11. This will be referenced as equation 1 within this paper. VImin and VImax are the maximum and minimum vegetation index values within the dataset. Fc is the calculated FoC. n is a calibrated exponent, often called the Choudhury exponent. The exponent was calibrated using the minimization of the sum of

square differences during the 2022 data. The exponent was then validated using fit and biases for the 2023 data.

$$F_C = 1 - \left[\frac{VI_{min} - VI}{VI_{max} - VI_{min}}\right]^n \quad (1)$$

Leaf Area Index

LAI was measured using a Plant Canopy Analyzer 2200 (LI-COR, Lincoln, Nebraska) in 2023. Collection dates were June 1, June 27, August 17, August 30, and October 14. The LAI data were split into calibration, Station 1, and validation, Station 2 datasets. Because of Station 2's mobility, two data points were sometimes collected on each data collection date (one point at the old location, one at the new). This gave Station 2 a more robust dataset with which to validate.

It is well-established that FoC and LAI are related to each other (Li, 2005). Camera-generated FoC was fit to observed LAI. The relationship between the two for Station 1, calibration, was validated against Station 2. Crop Height

Crop Height

Crop height at both stations was observed in 2022 and 2023. Each time a researcher was at the site, crop height measurements of grass and alfalfa were made. A composite crop height was calculated. The data were split into validation and calibration datasets. The 2022 data served as the calibration, and the 2023 data served as the validation. Relationships between FoC, LAI, NDVI, and crop height were evaluated. No apparent relationship existed. When crop height was compared to SAVI, a reasonable relationship was found.

Site Specific Inputs

There are several site-specific inputs in the TSEB model. Some of those were measured directly at the site. Those were the GPS coordinates, elevation, and sensor heights. Site spectral and canopy properties are also site-specific inputs. Spectral 19 properties were evaluated from commonly known ranges for our site's general description, ultimately the model’s default inputs were used. The canopy properties were also evaluated and ultimately the default values were also used.

There are a few different versions of the model available to the user. These deal with how temperature is partitioned within the model and the resistance model which deals with estimating the canopy boundary and soil resistances to heat and momentum transport. The options selected were the Priestly Taylor model with the Kustas-Norman resistance model (Kustas, 1999). The values used in the site-specific inputs are listed in Table 3.

Table 3

Site Specific PyTSEB Values

Input	Value
Latitude	40.46
Longitude	-109.56
Altitude (m)	1665.43
Temperature Measurement Height (m)	2.25
Wind Speed Measurement Height (m)	2.4
Leaf Visible Reflectance Parameter	0.07
Leaf Visible Transmittance Parameter	0.08
Leaf Near Infrared Reflectance Parameter	0.32
Leaf Near Infrared Transmittance Parameter	0.33
Soil Visible Reflectance Parameter	0.15
Soil Visible Transmittance Parameter	0.25
Soil Near Infrared Reflectance Parameter	0.98
Soil Near Infrared Transmittance Parameter	0.95
Maximum Canopy Transpiration	1.26
Soil Roughness	0.01
G to RN Flux Ratio	0.35
G Amplitude	0.35

Stations One and Two TSEB

PyTSEB was used to estimate energy fluxes for the canopy sensing data. The latent heat flux was used to calculate daily ET values. PyTSEB was run using the Jupyter Notebook platform. Station 1 and 2 data had input time steps of quarterly hours.

20 For data accuracy evaluation, Station 1 and 2 TSEB results were summed into hourly data and compared to the eddy covariance results. The eddy covariance tower is more appropriate to average on the hourly scale. Daily ET was then compared between the TSEB and eddy covariance results as well.

The data were broken into protected and unprotected sets. 2022 served as unprotected data. After running TSEB, several options were considered within this data. The ratio of soil heat flux to RN was altered, the albedo was lowered, and times of day, and seasonality were explored more independently. Ultimately the default values for the

soil heat flux to RN ratio and albedo were kept. Seasonality and time of day were found to play a factor within the TSEB results; however, it was decided to keep the dataset intact. Time of day and seasonality are discussed in the conclusion.

Landsat

The stations' sensor instrumentation and the eddy covariance tower had different footprint sizes. The proximal infrared temperature radiometer footprint was 0.79 m2 . Station 1 was very close to the tower, but never within its footprint. Station 2 was only in the tower's footprint at certain locations in 2023. To address the footprint size mismatch, PyTSEB was evaluated for Landsat imagery. Landsat has a pixel size between the stations and the eddy covariance footprint sizes and thus can serve as an intermediary. Pixels can also be evaluated in the wind direction to assess wind effects on the ET values.

The Jupyter Notebook platform was again used in the local image notebook. Local weather data were sourced from Station 1 and the eddy covariance tower for incoming solar radiation. FoC was calculated using Equation 1, NDVI was found using the Landsat bands for red and near-infrared. LAI was calculated using the derived 21 relationship between FoC and LAI. Crop height was evaluated from the found relationship to SAVI. SAVI was calculated from the Landsat red and near-infrared bands. Other site-specific options were left the same as for Station 1 and 2.

CHAPTER 4. RESULTS AND DISCUSSIONS

Bio-Physical Properties Results

Fraction of Cover

Data from 2022 were used as the calibration FoC dataset. Data from 2023 were used as the validation data. The 2022 Equation 1-derived FoC was compared to the 2022 camera-derived FoC. Data fit, and biases are listed in Table 4. The biases and overall goodness of fit were encouraging. The mean bias error (MBE, bias) in the calibration year was 3% high as a percentage of the mean. The overall fit (R^2) was 90%. In 2023, the validation year, the bias was 3% again but this time it was low. The overall goodness of fit improved to 93%. The root mean square error (RMSE) was low in both magnitude and as a percentage of mean. Unity between the two methods are shown in figures Figure 4 and Figure 5.

Table 4

2022 Calibration FoC Statistical Biases and Fit

Bias	2022 (Calibrate)		2023 (Validate)	
	Value (wm^{-2})	% of mean	Value (wm^{-2})	% of mean
RMSE	0.03	4%	0.08	11%
MBE	0.03	3%	-0.02	-3%
R^2	90%		93%	

Note: RMSE is Root Mean Square Error. MBE is Mean Bias Error.

Figure 4

2022 FoC Calibration Comparison

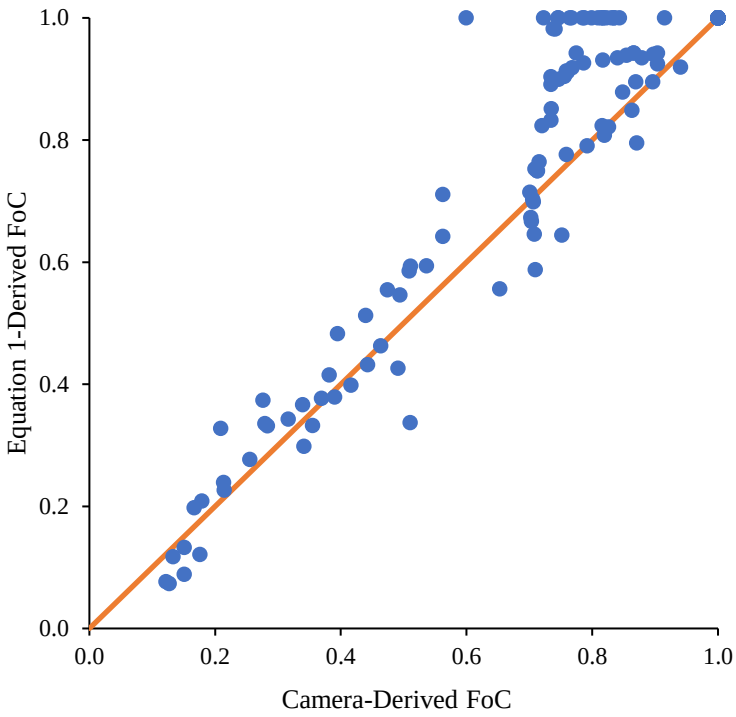

Note: The solid line represents unity (1:1).

Figure 5

2023 FoC Validation Comparison

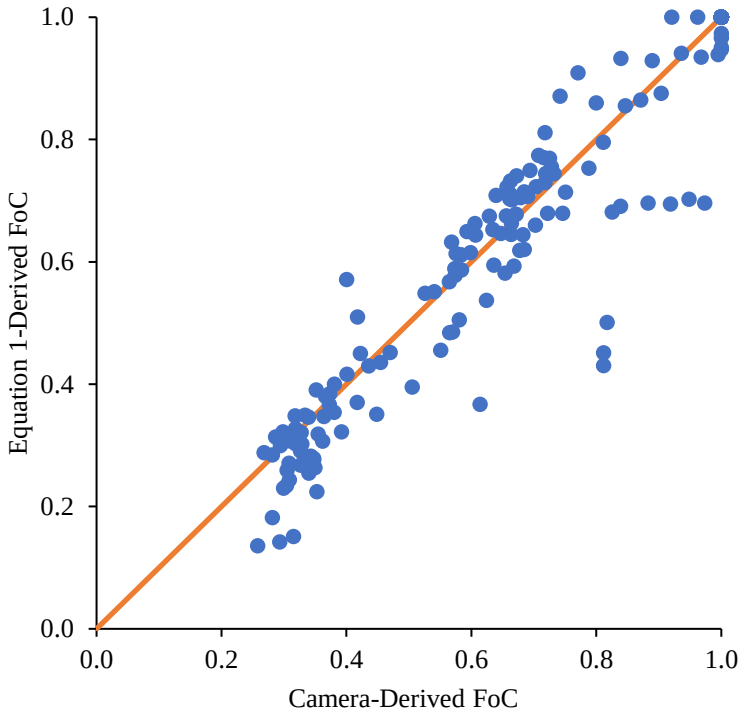

Note: The solid line represents unity (1:1).

One interesting trend the researchers observed was a “lag” between cuttings and a drop in Equation 1-generated FoC. Equation 1-generated FoC did not “drop off” exactly as the cutting happened, whereas in the visual-based camera-generated FoC, the “drop off” happened closer to the cutting. One possible explanation that was noticed was there was often cut vegetation within the footprints of the camera and the reflectance sensors. Within the code green vegetation, even cut, was treated as vegetation, while yellow vegetation was treated as “non-vegetation.” This can be seen more clearly within a timeseries comparison between the two methods of deriving FoC. Typically, this appeared as a small “u” shape after a cutting occurred in the timeseries plots; meaning

after the drop off from the cutting the FoC still went down for a few days until a local minimum, or the “bottom of the u” was reached. FoC then started to rise again. This is shown in Figure 26 through Figure 29 in the Appendix.

The camera method of determining FoC has the potential to eliminate the need for the red and near-infrared radiometers on the stations. This helps with station costs and implementation. Reducing the price point of the station is desirable for both management and research applications.

Leaf Area Index

The LAI relationship based on camera-generated FoC was evaluated against the measured LAI. Station 1 served as the calibration data to find the relationship. The Station 2 dataset was more robust and was used as the validation set. The relationship between the camera-generated FoC and LAI is displayed in Figure 6. This relationship is described in Equation 2.

Figure 6

Station 1 LAI Equation Development

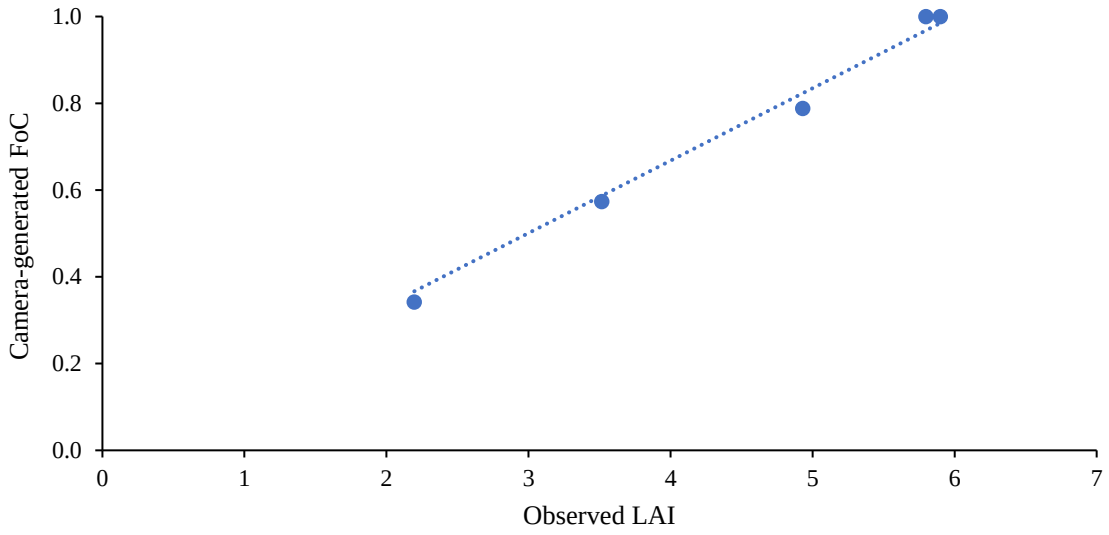

Note: The dashed line represents data linear best fit.

$$LAI = 6 * FoC \quad (2)$$

The mean bias error was negative for the calibration and validation datasets. This is evidence that the estimation of LAI through Equation 2 is lower than the observed. However, the MBE and the respective percentage of mean are low in magnitude.

The validation dataset had a larger bias in magnitude. It is important to note that the validation data represents Station 2 in 2023. In that year, Station 2 was moved to different locations. Due to the site-specific nature of Equation 2, larger biases and poorer fit are expected for the validation data. Table 5 is a list of the summary of the biases and fit for LAI, Figure 7 is a plot of modeled vs. measured LAI for the validation data.

Table 5

LAI Biases and Fit

Bias	Calibration		Validation	
	Value (wm^{-2})	% of mean	Value (wm^{-2})	% of mean
RMSE	0.15	3.5%	0.77	16%
MBE	-0.024	-0.55%	-0.40	-8.3%
R^2	99%		77%	

Note: RMSE is Root Mean Square Error. MBE is Mean Bias Error.

Figure 7

Leaf Area Index Validation Comparison

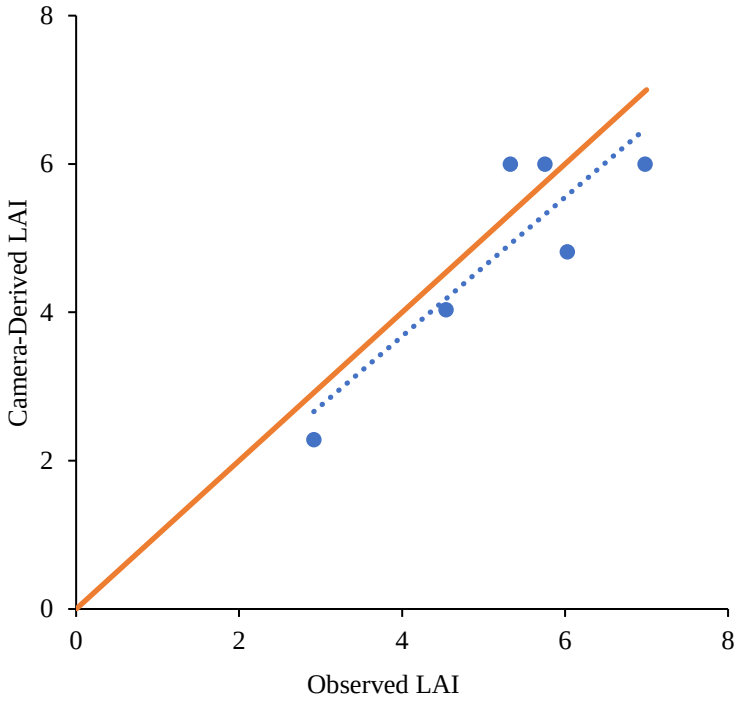

Note: The sold line represents unity (1:1). The dotted line represents data linear best fit.

Crop Height

Crop height was estimated from a relationship found between observed measurements and SAVI. The 2022 data were used as the calibration dataset, and the 2023 data were used as the validation dataset. This is displayed in Figure 8. Equation 3 was then used to calculate crop height for the entire timeseries and compared against the measured heights.

Figure 8

Crop Height Equation Development

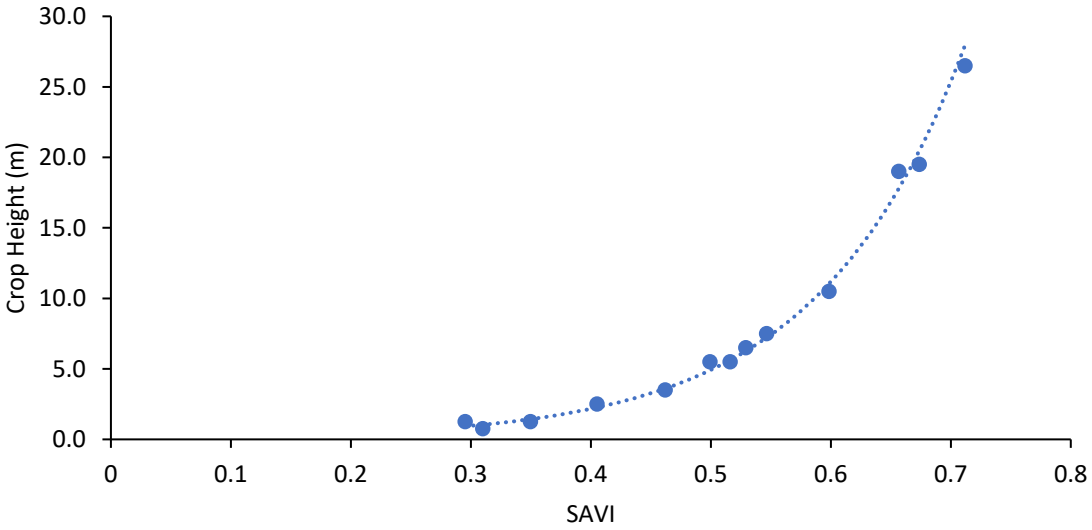

Note: The dotted represents data exponential best fit.

$$\text{Crop Height (m)} = 0.08e^{8.2\text{SAVI}} \quad (3)$$

A plot of the modeled verses crop height values approached unity for both years. The fit and the bias of both datasets were encouraging. The summary of this is displayed in Table 6. It is good to note the validation data was collected during the period when Station 2 was being moved to various locations. Due to the site-specific nature of

Equation 3, this is to be expected. Validation modeled and measured values are presented in Figure 9.

Table 6

Crop Height Biases and Fit

Bias	Calibration		Validation	
	Value (wm^{-2})	% of mean	Value (wm^{-2})	% of mean
RMSE	0.02	7%	1.20	14%
MBE	0.003	1%	0.07	-1%
R2	99%		95%	

Note: RMSE is Root Mean Square Error. MBE is Mean Bias Error.

Figure 9

Crop Height Validation Comparison

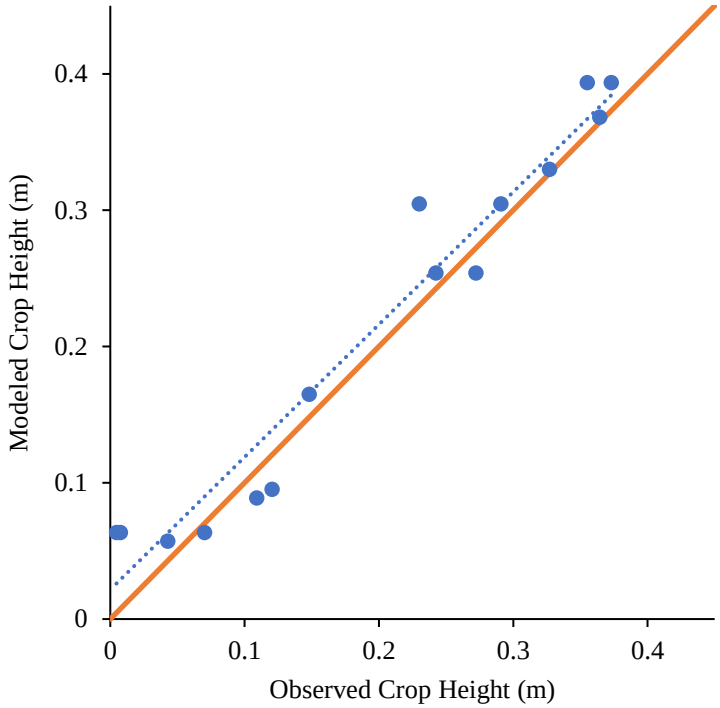

Note: The solid line represents unity (1:1). The dotted line represents data linear best fit.

PyTSEB

Unprotected

PyTSEB finds the flux for each of the four components of the energy balance: RN, G, H, and LE. The unity for those four components of the unprotected data is displayed in Figure 10 through Figure 13. The statistical biases and overall fit are in Table 7.

Table 7

Calibration Data Biases and Fit

Bias	**RN**		**H**	
	Value (wm^{-2})	% of Mean	Value (wm^{-2})	% of Mean
RMSE	104	29%	64	-4181%
MBE	24	7%	-35	2288%
R^2	75%		31%	
Bias	**G**		**LE**	
	Value (wm^{-2})	% of Mean	Value (wm^{-2})	% of Mean
RMSE	40	85%	159	50%
MBE	12	25%	101	32%
R^2	16%		63%	

Note: RMSE is Root Mean Square Error. MBE is Mean Bias Error.

Figure 10

2022 Modeled and Measured RN

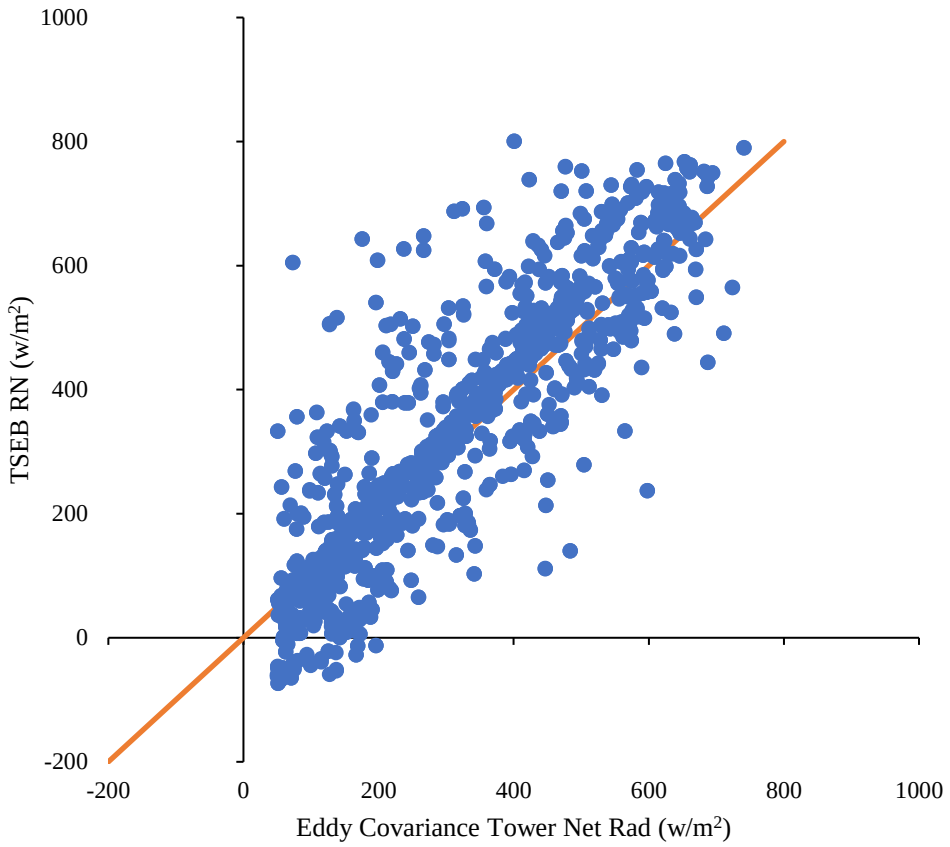

Note: The solid line represents unity (1:1).

The bias for the unprotected RN was 7% high. Within the RN data there were several data "families" that were identifiable. The data "family" near the unity line was nearer the line when RN was below about 400 W m^{-2}. After that, the data "family" was greater than the unity line. There seemed to be another "family" of data that is less than the unity line above the 400 W m^{-2} threshold. However, this family has fewer data points.

There is some scatter away from unity in the RN. The scatter is both low and high, but there is a larger amount of data points scattered high.

Figure 11

2022 Modeled and Measured G

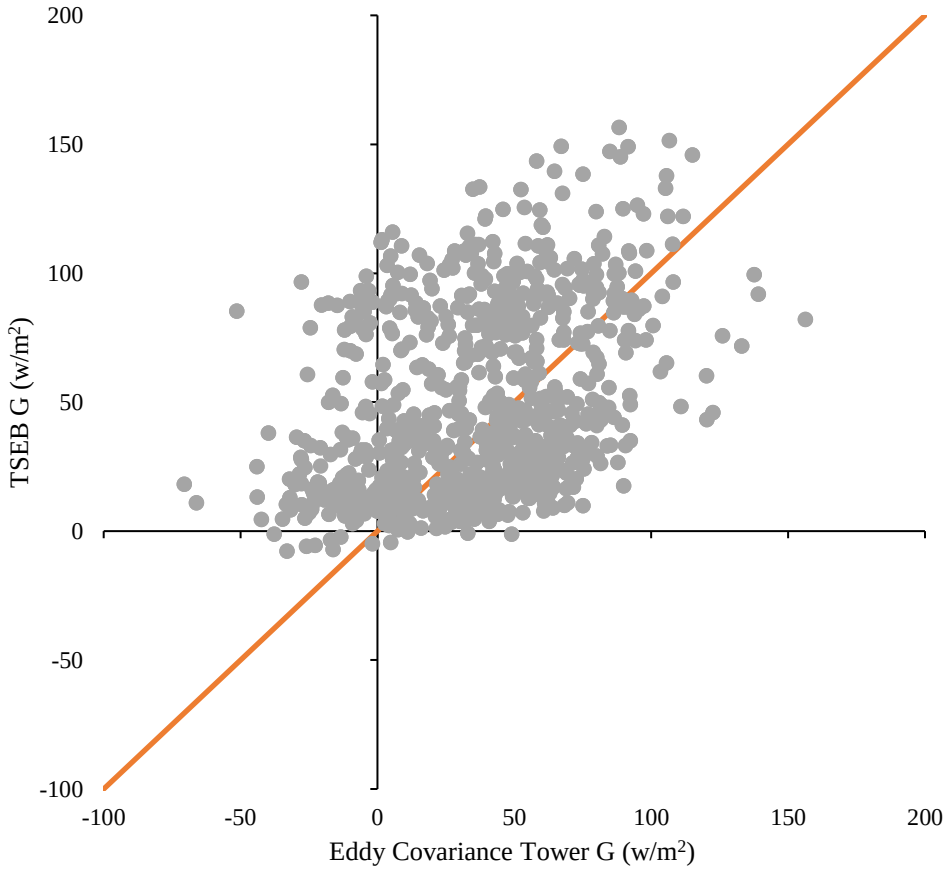

Note: The solid line represents unity (1:1).

The bias in G was 25% high. It is not necessarily appropriate to evaluate the biases as a percentage of the mean. This is due to the mean being low. A more appropriate analysis is to look at the magnitude of the biases.

When eddy covariance G was used with hourly canopy sensing data, the LE and ET values had negative bias low. This is evidence that G as a constant percentage of Rn throughout the day produces a low estimate of G. Great percentages of G to RN were calculated. These had negligible effects on LE, indicating model G was biased low but inconsistently so.

Figure 12

2022 Modeled and Measured H

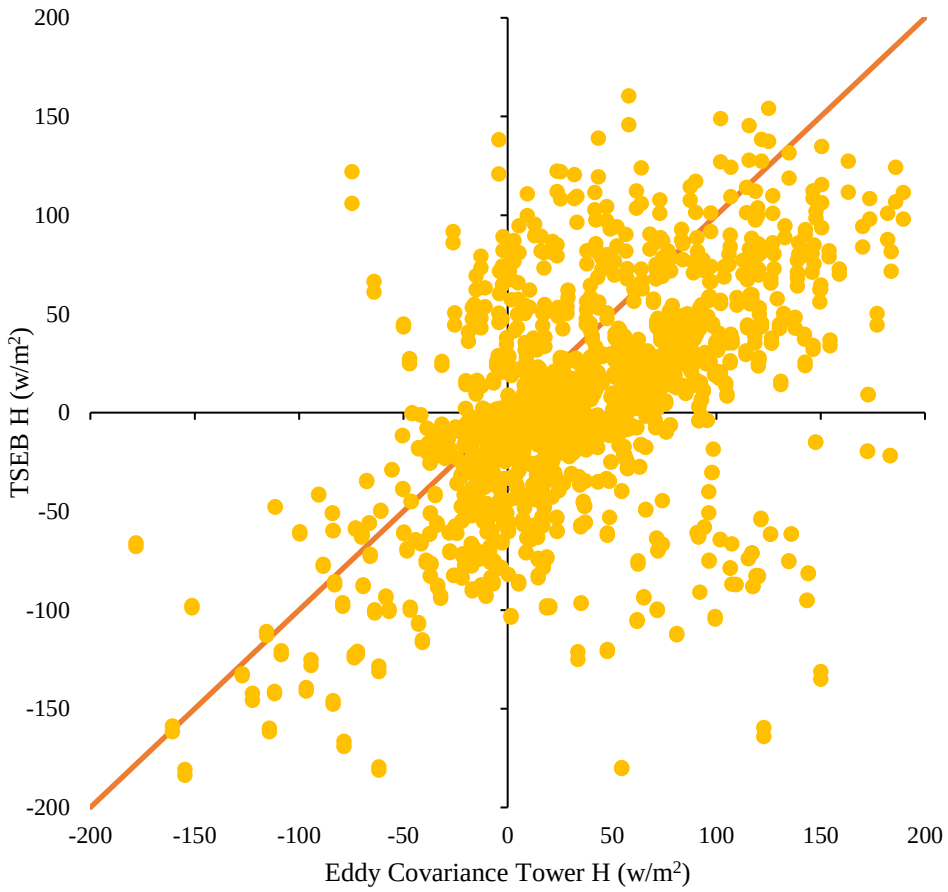

Note: The solid line represents unity (1:1).

Similar to G, the biases of H are not necessarily appropriate to be evaluated as a percentage of the mean. This is because the mean is very small. The magnitude of the

biases is a more appropriate method of analysis. The bias is low by 35 W m^{-2}. The RMSE value is 64 W m^{-2}.

Figure 13

2022 modeled and measured LE

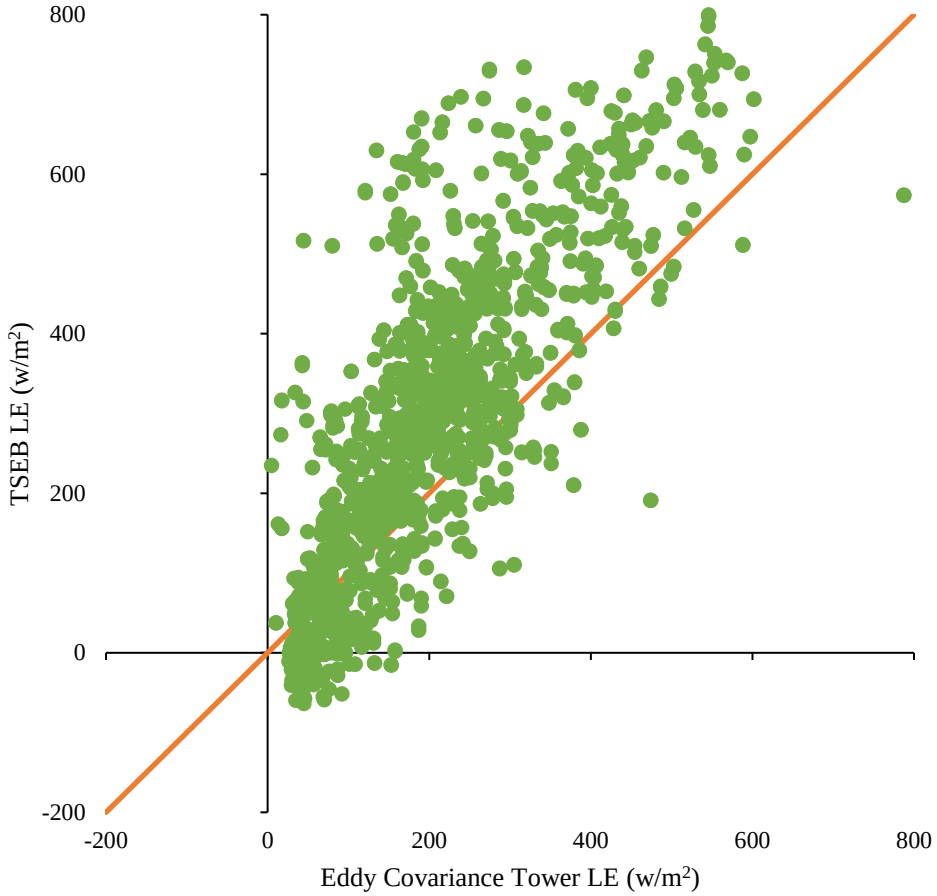

Note: The solid line represents unity (1:1).

The bias in LE is 32 %high. LE unity was low when the magnitude of LE was lower. LE unity was higher when the magnitude of LE was high. The scatter for LE increased as LE increased in magnitude.

Several methods were undertaken to see if the bias in the LE and H fluxes could be reconciled. During solar noon, the sun angle is closest to directly above the station.

This has fewer shadow effects on the sensors. Data near solar noon were extracted and evaluated by themselves. This resulted in improvements in bias and fit for Rn, H, and G. The fit and bias for LE were less desirable than the entire timeseries dataset. Biases and fit of solar noon are listed in Table 8. A comparison of modeled and measured energy fluxes near solar noon calibration unity is in Figure 14.

Table 8

Solar Noon Calibration Data Biases and Fits

Bias	**RN**		**H**	
	Value (wm^{-2})	% of Mean	Value (wm^{-2})	% of Mean
RMSE	79	15%	77	1398%
MBE	40	8%	-58	-1046%
R^2	79%		41%	
Bias	**G**		**LE**	
	Value (w/m2)	% of Mean	Value (wm^{-2})	% of Mean
RMSE	37	57%	193	43%
MBE	-0.1	-0.1%	165	37%
R^2	18%		60%	

Note: RMSE is Root Mean Square Error. MBE is Mean Bias Error.

Figure 14

Station 1 and 2 2022 Solar Noon Calibration Energy Summary

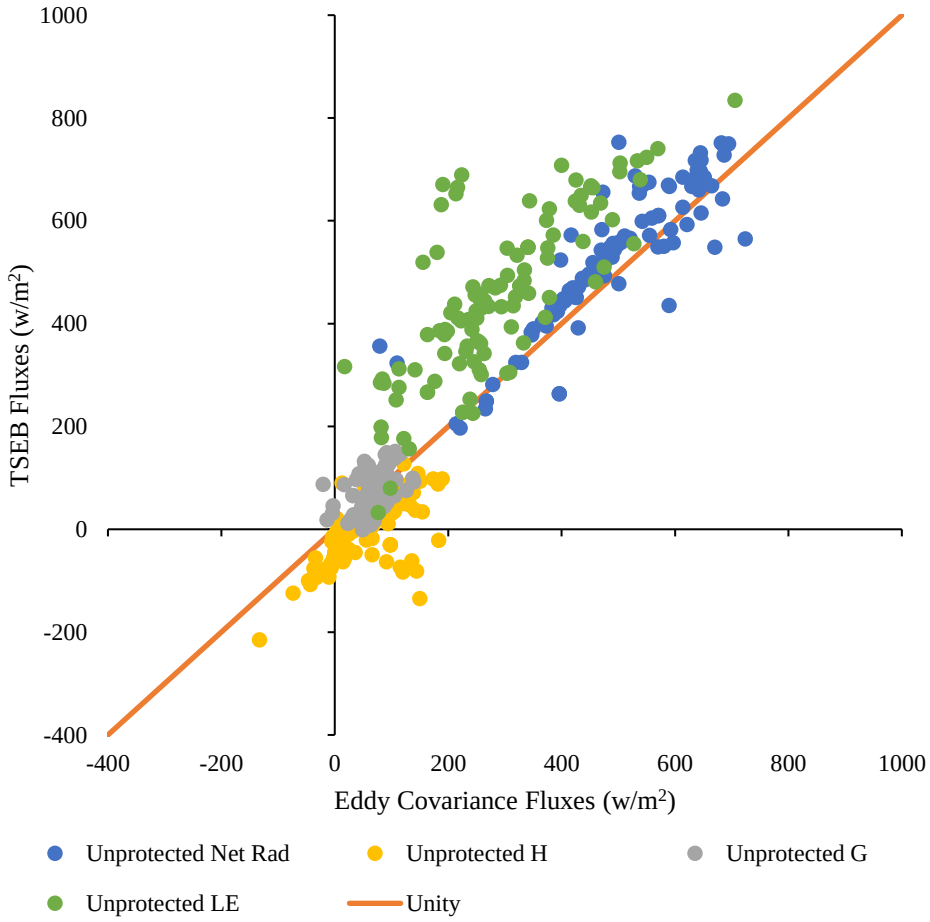

Clear-day radiation (RSO) was computed. This was plotted against incoming shortwave radiation, and potentially cloudy days were identified. For these days, the data were ignored, and the new dataset was re-evaluated. This visually improved the comparison plot graph but had a minor impact on the fit statistics. Several thresholds were set for the percent difference between RSO and incoming shortwave radiation; data points above the threshold were ignored. This again improved the appearance of the

comparison plot but had negligible effects on the bias and fit. Hourly RSO calculations and incoming shortwave timeseries are in Fig. 31 in the Appendix.

The model was rerun after averaging the quarter-hourly input data into hourly values for comparison with the eddy covariance data. The LE bias had only a slight change in magnitude. Hourly data were evaluated with G as an input from the eddy covariance tower instead of using the modeled values. This again resulted in only minor improvements in the magnitude of the LE bias. Hourly LE fluxes with eddy covariance G are shown in Figure 32 in the Appendix.

Weather input data were also evaluated between Station 1 and the eddy covariance tower. Weather data were compared for different times of day and seasonality. No significant deviations were found in this comparison. Plots of Station 1 versus eddy covariance system air temperature and vapor pressure are shown in Fig. 34 and Figure 35 respectively.

For the purpose of footprint size comparisons, the energy fluxes modeled from the available Landsat imagery were compared against those from Station 1, Station 2, and the eddy covariance data at the same time points. The comparison statistics for this analysis are in Table 9 and Figure 15. Significant improvement in H and G biases and H fit is noted.

Table 9

Landsat biases and fit to eddy covariance tower

Bias	**RN**		**H**	
	Value (wm^{-2})	% of mean	Value (wm^{-2})	% of mean
RMSE	91	16%	41	146%
MBE	86	15%	-30	-108%
R^2	54%		64%	
Bias	G		LE	
	Value (wm^{-2})	% of mean	Value (wm^{-2})	% of mean
RMSE	47	60%	204	45%
MBE	13	17%	187	41%
R^2	0.021%		50%	

Note: RMSE is Root Mean Square Error. MBE is Mean Bias Error.

Figure 15

Modeled Calibration Dataset Energy Fluxes for Landsat, Stations 1 and Station 2

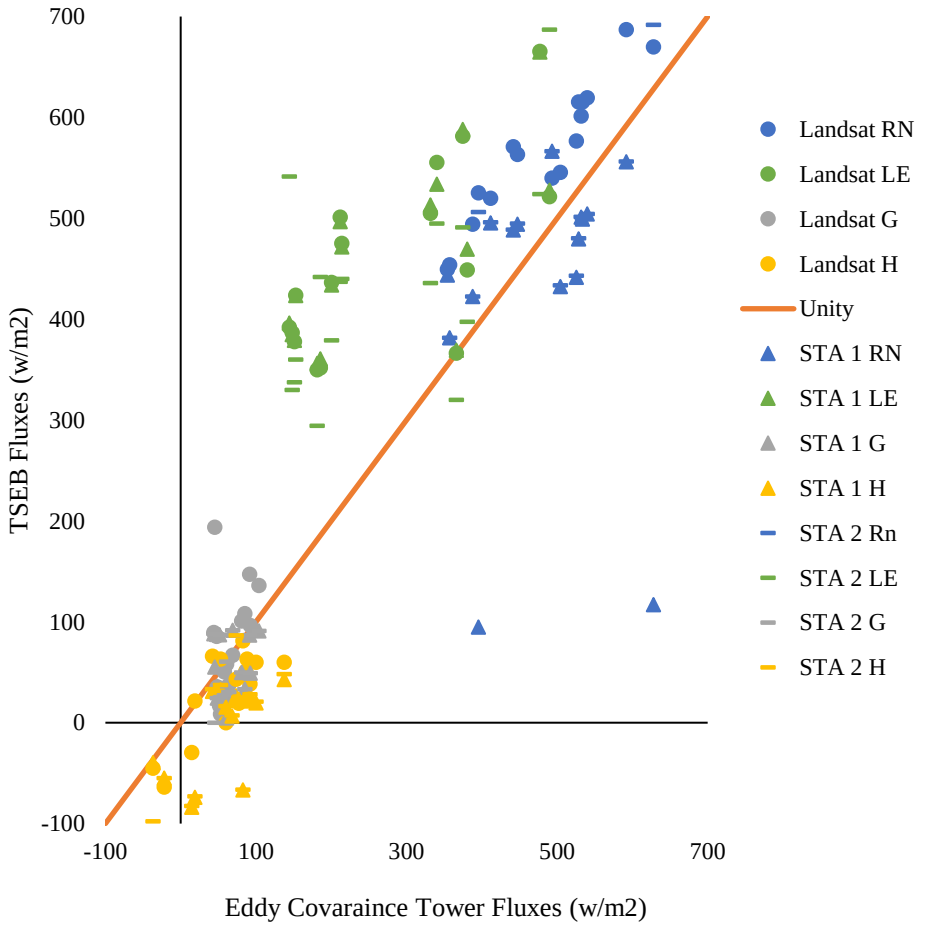

When dealing with grower management, the daily ET value is often the number used to manage the crop properly. The daily ET values of the calibration data are plotted against the eddy covariance values in Figure 18. It must be noted that these values are not representative of the entire day. The data points which the net radiometer fell below 50 W m^{-2} were filtered out. his typically filtered out nighttime hours. Some cloudy days were also filtered out. Some insufficient data also existed due to challenges with the stations' battery system. These points were filtered out. The time in which the Station users were

underneath the station for maintenance were also filtered out. Data gap filling occurred when a day had daytime hourly data with gaps 2 hours or less. Reference ET was calculated for the data gaps. A ratio of the TSEB to Reference ET values for the timestep before and after the gap was applied to the reference ET value of the gap. Even with these points filtered out, the ET values follow the general trend of the ET values from the eddy covariance tower.

Eddy covariance technology does not force closure on the energy balance (RN = H+G+LE). The TSEB model forces closure. This can make a significant difference in the comparisons. The research team which ran and maintained the eddy covariance tower calculates daily closure on the energy balance after the energy balance has been processed every year. It is not necessarily appropriate to compare the closed and unclosed values. The closure ratio was applied to the ET values for the eddy covariance tower results before comparison.

The ET biases and fit are displayed in Table 10. The timeseries between the two stations' ET values is explored in Figure 16 and Figure 17. The vertical lines represent the cutting dates. The overall fit was 86%. One interesting trend the researchers observed was that the end of season ET was responsible for the majority of the bias. In October, the bias responded in a similar pattern to the eddy covariance values but was biased high. We were unable to identify the cause of this increased bias. Camera-generated FoC tended to be higher than the equation 1-generated FoC, near the end of the growing season. This was explored as a possible explanation. No correlation was found. Further refinement will be the focus of future research. The unity is displayed in Figure 18.

Table 10

Daily ET Values Biases and Fit

	Station 1		Station 2	
	Value (wm^{-2})	% of Mean	Value (wm^{-2})	% of Mean
RMSE	0.9	22%	0.9	22%
MBE	0.6	15%	0.6	15%
R^2	86%		86%	

Note: RMSE is Root Mean Square Error. MBE is Mean Bias Error.

Figure 16

2022 Station 1 ET Timeseries

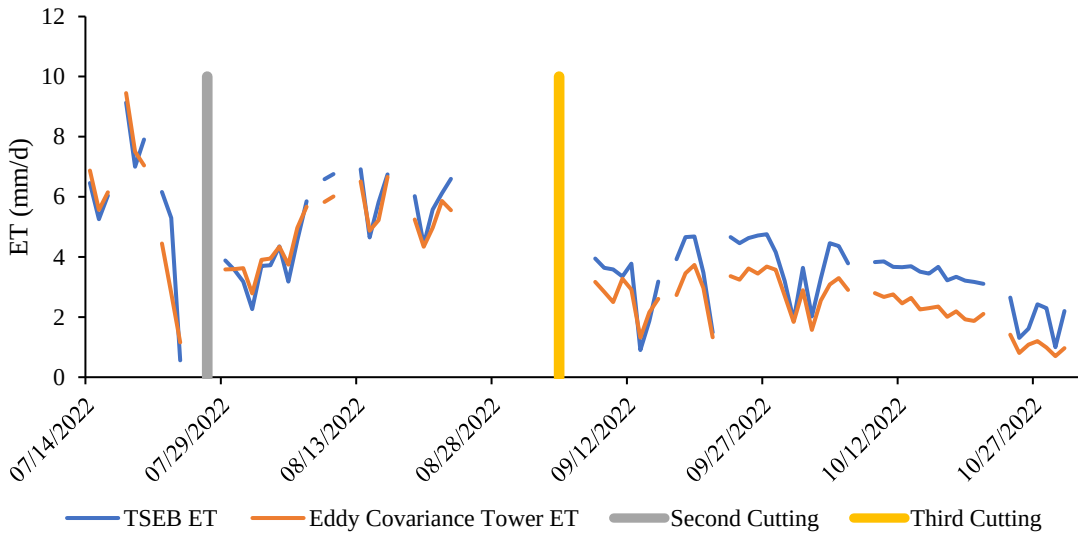

Figure 17

2022 Station 2 ET Timeseries

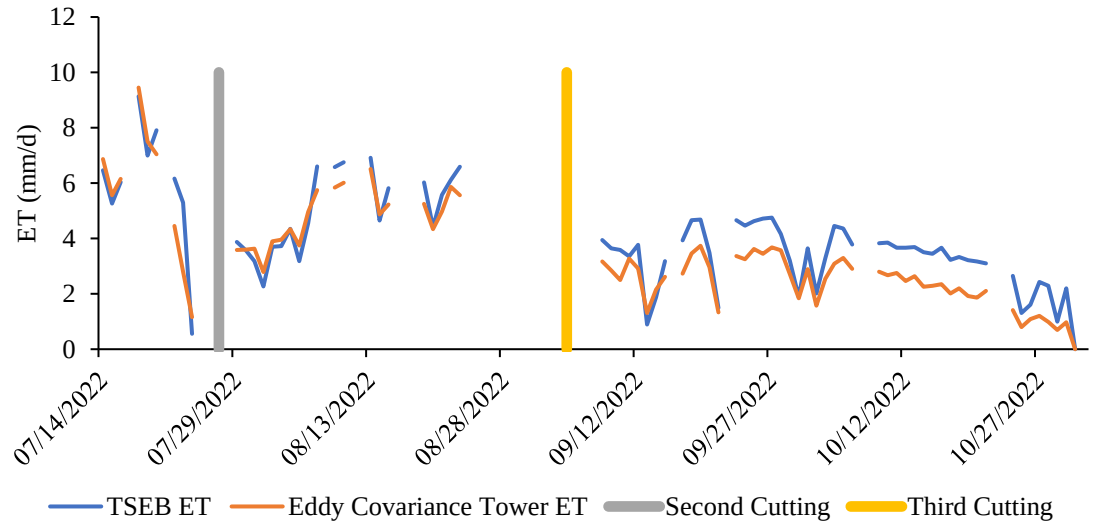

Figure 18

2022 Modeled and Measured ET

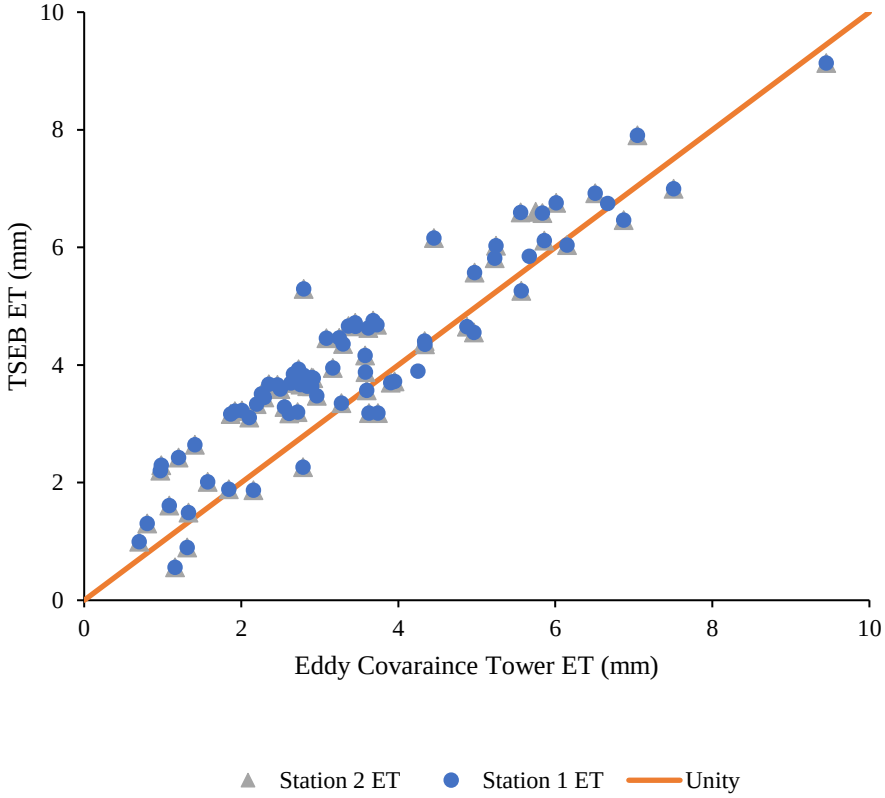

When compared to similar work (Colaizzi, 2012a) TSEB results are also seen to be higher than observed. In that study, corn and cotton ET values were a similar percentage biased than the forced closure 2022 TSEB ET results. Some other TSEB work that involves mobile non continuous monitoring that use a temporal scaling to find daily ET includes Katimbo (2022b). That study found ET to be overestimated by a bias range of 0.2- and 1.6-mm d^{-1}. The bias of the 2022 forced closure of the present study fell within this range at 0.6 mm d^{-1}.

Protected

The 2023 data were protected from any of the aforementioned methods of reconciling bias. The 2023 data were analyzed the exact same way the 2022 data were ultimately done. The biases and fit of the 2023 data are displayed in Table 11. The energy summary unity is displayed in Figure 19 through Figure 22.

Table 11

2023 Data Biases and Fit

Bias	**RN**		**H**	
	Value (wm^{-2})	% of mean	Value (wm^{-2})	% of mean
RMSE	120	34%	57	1193%
MBE	0.3	0.1%	-28	-577%
R^2	69%		26%	
Bias	G		LE	
	Value (wm^{-2})	% of mean	Value (wm^{-2})	% of mean
RMSE	42	129%	178	56%
MBE	-5	-16%	107	33%
R^2	14%		47%	

Note: RMSE is Root Mean Square Error. MBE is Mean Bias Error.

Figure 19

2023 Modeled and Measured RN

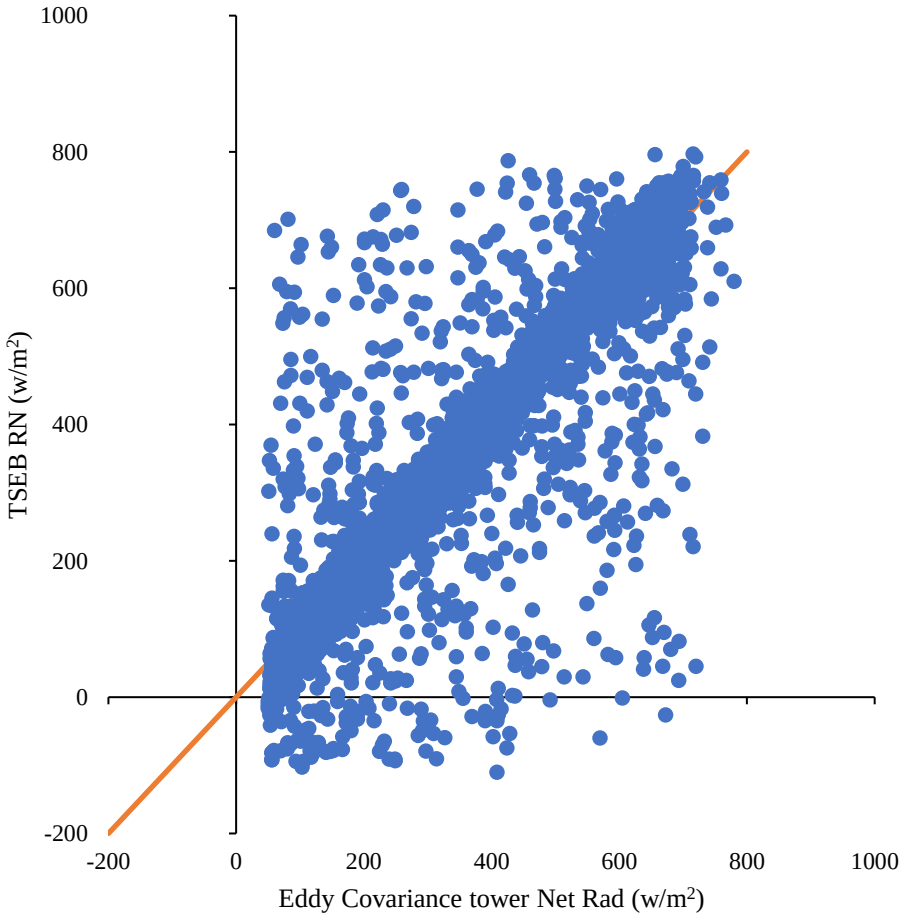

Note: The solid line represents unity (1:1).

The bias in the protected RN is lower than that of the unprotected. The bias is near 0. However, the protected RN data have the bulk of the points falling on or very near the unity line. No discernable “families” are seen like those in the unprotected data. There is a larger visible spread, this is partially because there are more data points. Even so, taking this into account the spread is wider within the protected data.

Figure 20

2023 Modeled and Measured H

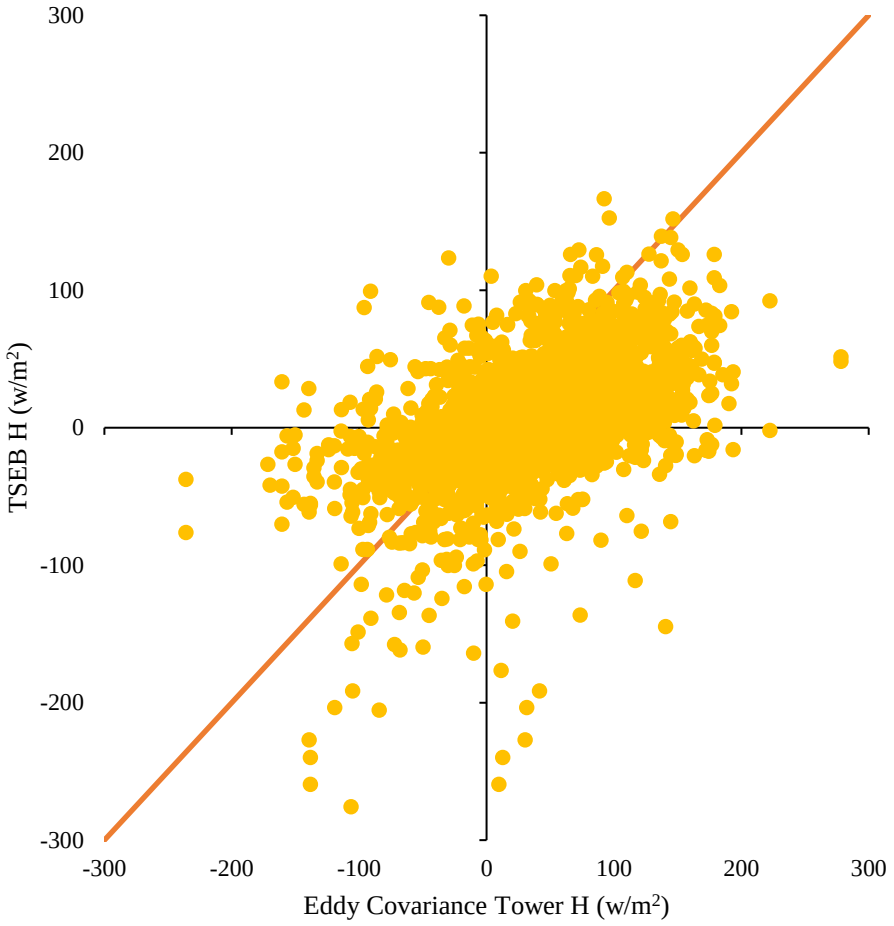

Note: The solid line represents unity (1:1).

The biases in H are quite large as a percentage of their mean. However, this again is not necessarily an appropriate way to evaluate these data. Both the MBE and the RMSE are less in magnitude compared to the unprotected data.

Figure 21

2023 Modeled and Measured G

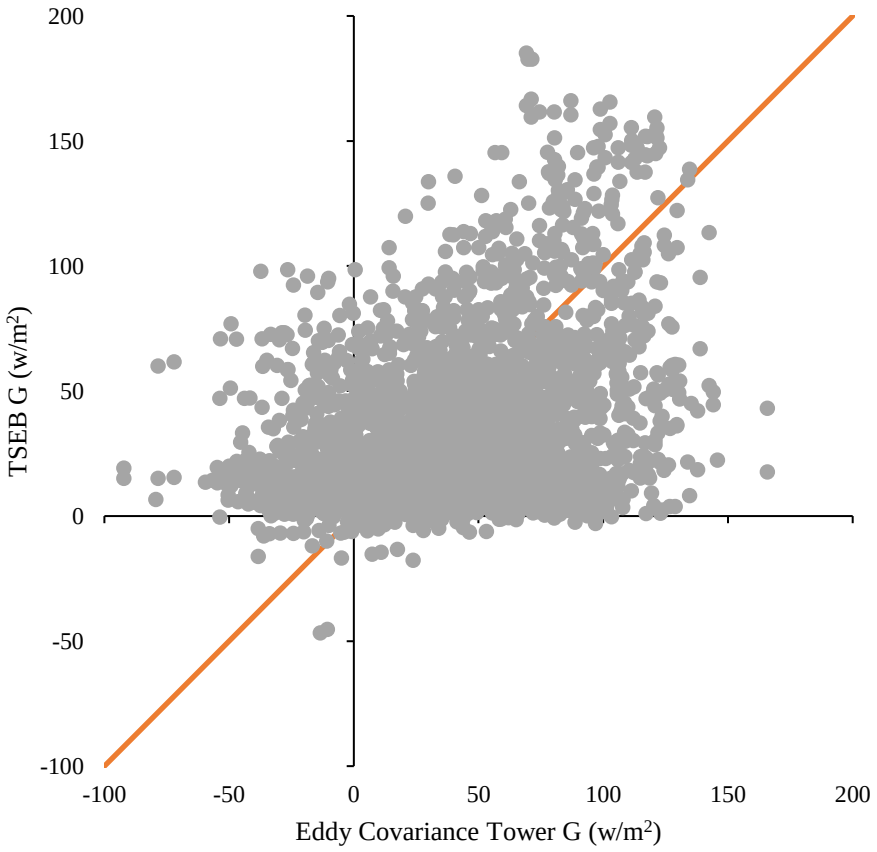

Note: The solid line represents unity (1:1).

The biases as a percentage of the mean are also high for G, but again this is not necessarily an appropriate evaluation method. The MBE is lower in magnitude than the unprotected G, indicating lower average bias. However, the RMSE is larger indicating that G is not being predicted by the model as well.

Figure 22

2023 Modeled and Measured LE

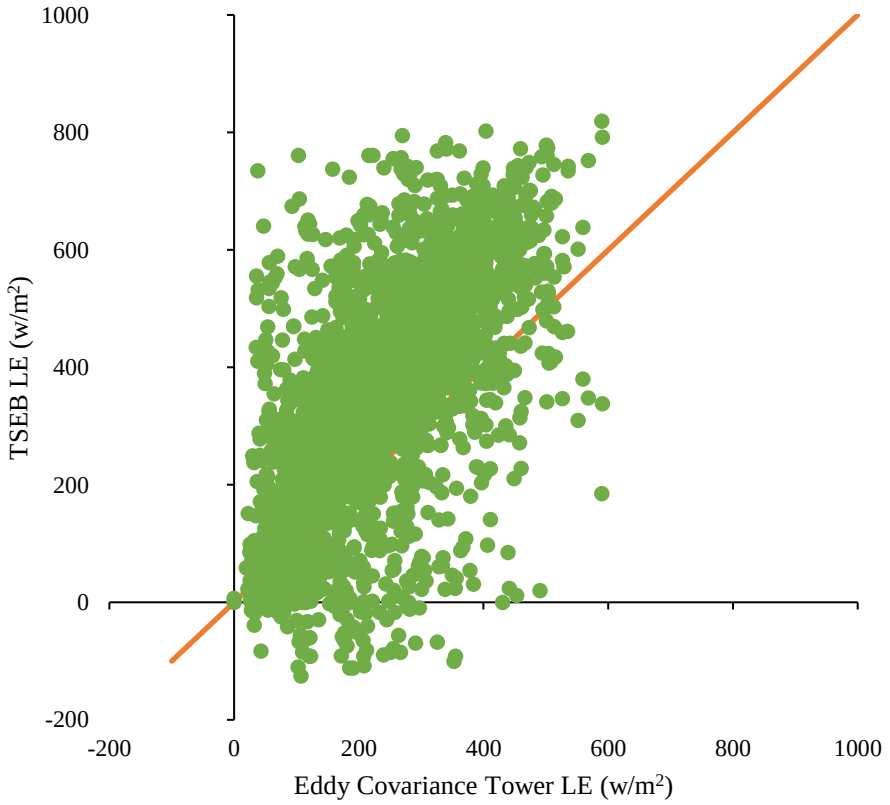

Note: solid line represents unity (1:1).

The biases for LE were very similar to that for the unprotected data. Daily ET values were computed from the protected hourly LE values. It is important to note that these ET values only represent daytime hours when data were collected and not disregarded as described for the calibration data. The gap filling process was the same as well. The biases and fit of the daily ET values are presented in Table 12. The daily ET

timeseries are displayed in Figure 23 and Figure 24. The daily Unity ET is displayed in Figure 25.

Table 12

Validation daily ET biases and fit.

Bias	**Station 1**		**Station 2**	
	Value (wm^{-2})	% of Mean	Value (wm^{-2})	% of Mean
RMSE	2	37%	2	40%
MBE	1	31%	2	37%
R^2	66%		75%	

Note: RMSE is Root Mean Square Error. MBE is Mean Bias Error.

Figure 23

2023 Station 1 and Eddy Covariance ET Timeseries

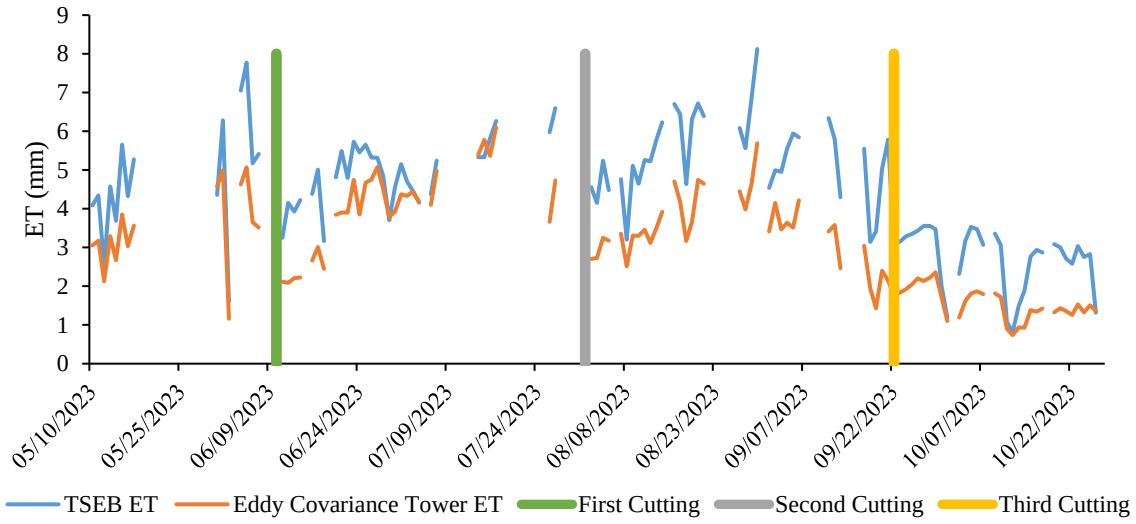

Figure 24

2023 Station 2 and Eddy Covariance ET Timeseries

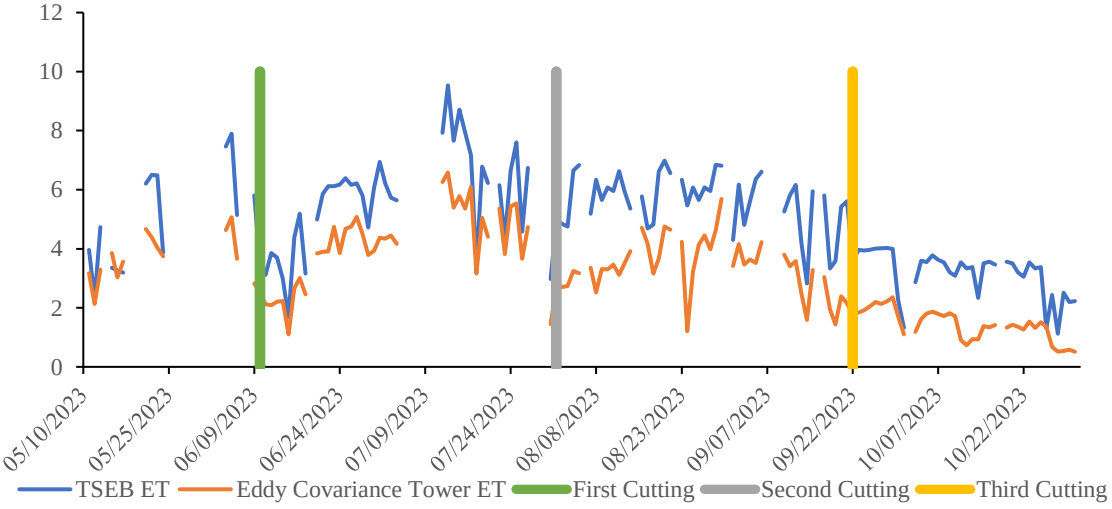

Figure 25

2023 Modeled and Measured ET

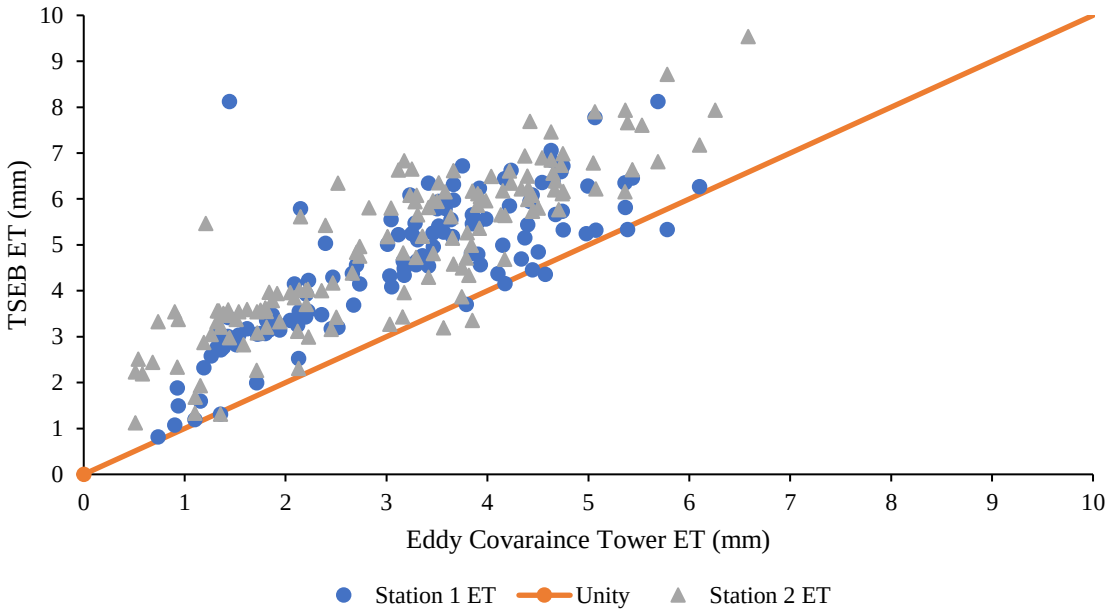

Closure data had not been processed for the 2023 growing season. From the historical data of the site, a similar change in bias is expected in 2023 that was seen in 2022. It was observed that the station data were not as similar between stations as compared to the 2022 data. This is expected because 2023 was the time period in which Station 2 was moved around to different locations within the field. The bias was double for the protected dataset. The unprotected data were compared against forced closure eddy covariance tower data. This decreased the bias from the LE bias for the unprotected data. The protected data bias is the same as the LE bias. The RMSE was lower for the unprotected data indicating better prediction. Again, closure being forced on the unprotected data lowered the RMSE, while closure for the 2023 eddy covariance tower data was not forced.

Chapter 5. CONCLUSIONS

Research Objective Tasks

Data Collection

The implementation of the canopy sensing station prototypes was deemed viable for this task. As with any prototype, this was not without challenges.

Biophysical properties

The biophysical properties modeled for the TSEB process had promising results. Modeling FoC from camera photography reduces the need for the red and near-infrared radiometers. This decreases station price point and maintenance needs. The accuracy of FoC from the stations' photography compared well against Equation 1 methods.

LAI modeling from FoC can reduce the station's need for LAI data collection visits. This can also reduce the labor and price point of the station. This method validated well against observed LAI. The TSEB model is very sensitive to LAI, so LAI validation is of utmost importance. It is good to note that the LAI equation was site specific so for future implementation, LAI data would need to be collected in order for the exact relationship for that application to be found (Gao, 2022).

The station crop height was validated well using the relationship found between SAVI and observed measurements. This requires the use of red and near-infrared radiometers. Methods to calculate crop height that do not require the red and near infrared radiometers are discussed in the future applications section. Overall, the part of this sub-objective dealing with modeling the biophysical properties was deemed viable.

TSEB and ET

TSEB modeling had mixed results. In the protected and unprotected hourly data, RN had low biases and tight fit. This is similar to other work using the TSEB model (Colaizzi, 2014; Liang, 2021). LE was biased high for the hourly data. This bias was larger than desired. One recognizable trend was that LE tended to be low in the morning and late evenings but high in the middle of the day. Coupling this with the solar noon calibration data, where LE had greater bias, seems to indicate that LE is overestimated around solar noon.

ET values follow the general trend of the eddy covariance ET. This is evidence that TSEB modeled the interseason relative differences correctly. Forcing closure on ET for the eddy covariance tower reduced bias from the LE flux to the ET calculations. This reduction in bias is expected to be similar for the protected 2023 data. This indicates that the TSEB model is performing better than the flux data indicated. However, the bias is still high

Research Objective

The research objective of accurately modeling plot-scale ET using the TSEB model with continuous ground based remote sensing technology had some components that were successful, some that were unsuccessful, and some that need further evaluation. The modeling of ET using the TSEB model with continuous ground based remote sensing methods was a success. The continuous portion of the research objective was unsuccessful. However, there were less gaps in the data in 2023. Indicating that as methods become more refined, continuous monitoring is possible. The model was 50

extremely accurate in some places and significantly differed from the eddy covariance tower results in other places.

Future Applications and Recommendations

This station setup has the potential to be used to estimate ET at a low cost and a manageable scale. Further work with similar stations is planned. Stations also included soil moisture and matric potential sensors that were not used in this research. Further work involving a comparison between water balance and TSEB-calculated ET is possible.

Recommendations and improvements for several aspects of the research exist. Using multiple cameras, photogrammetry can be used to calculate crop. Thus, eliminating the need for the red and near-infrared radiometers. The time required to process the images to find FoC through the code written is extensive. Machine learning and memory could be adapted into the code so classifications are remembered and can be predicted with training.

There exist possibilities for management applications for the stations. Implementation in field plots for treatment analyzing is a possibility. Analyzing real time ET for plots of high value crops or areas of production issues is another possible application that has been discussed.

References

Allen, R., Irmak, A., Trezza, R., Hendrickx, J.M.H., Basstiaanssen, W., Kjaersgaard, J. (2011). Satellite-based ET estimation in agriculture using SEBAL and METRIC. *Hydrological Processes,* 25, 4011 – 4027. doi: 10.1002/hyp.8408

Allen, R.G., Tasumi, M., Trezza, R. (2007). Satellite-based energy balance for mapping evapotranspiration with internalized calibration (METRIC) – model. *Journal of Irrigation and Drainage Engineering,* 133(4), 380-394. doi: 10.1061/(ASCE)0733-9437(2007)133:4(380)

Anderson, M.C., Neale, C.M.U., Li, F., Norman, J.M., Kustas, W.P., Jayanthi, H., Chavez, J. (2004). Upscaling ground observations of vegetation water content, canopy height, and leaf area index during SMEX02 using aircraft and Landsat imagery. *Remote Sensing of Environment,* 92, 447–464. doi: 10.1016/j.rse.2004.03.019

Barker, J. B., Neale, C. M. U., Heeren, D. M., and Suyker A. E. (2018). Evaluation of a hybrid reflectance-based crop coefficient and energy balance evapotranspiration model for irrigation management. *Transactions of the ASABE* 61(2): 533-548. doi: 10.13031/trans.12311.

Bastiaanssen, W.G.M., Menenti, M., Feddes, R.A., Holtslag, A.A.M. (1998). A remote sensing surface energy balance algorithm for land (SEBAL) 1. Formulation. *Journal of Hydrology,* 212-213, 198-212. doi: 10.1016/S0022-1694(98)00254-6

Bausch, W.C., Neale, C.M.U. (1987). Crop coefficients derived from reflected canopy radiation: A Concept. *Transactions of the ASCE,* 30(3), 703-709. doi: 10.1061/(ASCE)IR.1943-4774.0001309

Bausch, W.C. (1995). Remote Sensing of Crop Coefficients for Improving the Irrigation Scheduling of Corn. *Agricultural Water Management,* 27, 55–68.

Berni, J.A.J., Zarco-Tejada, P.J., Suárez, L., Fereres, E. (2009). Thermal and Narrowband Multispectral Remote Sensing for Vegetation Monitoring from an Unmanned Aerial Vehicle. *IEEE Transactions on Geoscience and Remote Sensing*, 47(3). doi: 10.1109/TGRS.2008.2010457

Bellvert, J., Jofre-Ĉekalović, C., Pelechá, A., Mata, M., Nieto, H. (2020). Feasibility of Using the Two-Source Energy Balance Model (TSEB) with Sentinel-2 and Sentinel-3 Images to Analyze the Spatio-Temporal Variability of Vine Water Status in a Vineyard. *Remote Sensing*, 12. doi: 10.3390/rs12142299

Briggs, L.J., Shantz, H.L. (1914). Relative Water Requirement of Plants. *Journal of Agricultural Research,* 3 (1), 1–65.

Colaizzi, P.D., Agam, N., Tolk, J.A., Evett, S.R., Howell, T.A., Gowda, P.H., O'Shaughnessy, S.A., Kustas, W.P., Anderson, M.C. (2014). Two-Source Energy Balance Model to Calculate E, T, And ET: Comparison of Priestley-Taylor and Penman-Monteith Formulations and Two Time Scaling Methods. *Transactions of the ASABE,* 57(2), 479–498. 10.13031/trans.57.10423

Colaizzi, P.D., Agam, N., Tolk, J.A., Evett, S.R., Howell, T.A., O'Shaughnessy, S.A., Gowda, P.H., Kustas, W.P., Anderson, M.C. (2016). Advances in a two-source energy balance model: Partitioning of evaporation and transpiration for Cotton. Transactions of the ASABE, 59(1), 181–197. https://doi.org/10.13031/trans.59.11215.

Colaizzi, P.D., Evett, S.R., Howell, T.A., Gowda, P.H., O'Shaughnessy, S.A., Tolk, J.A., Kustas, W.P., Anderson, M.C. (2012a). Two-Source Energy Balance Model: Refinements and Lysimeter Tests in The Southern High Plains. *Transactions of the ASABE,* 55(2), 551–562, doi: 10.13031/2013.41385

Colaizzi P.D., Kustas, W.P., Anderson, M.C., Agam, N., Tolk, J.A., Evett, S.R., Howell, T.A., Gowda, P.H., O'Shaughnessy, S.A. (2012b). Two-source energy balance and model estimates of evapotranspiration using component and composite surface temperatures. *Advance in Water Resources,* 50, 14–151, https://doi.org/10.1016/j.advwatres.2012.06.004

Choudhury, B. J., Ahmed, N. IJ., ldso, S. B., Reginato, R. J., and Daughtry, C. S. T. (1994). Relations between evaporation coefficients and vegetation indices studied by model simulations. *Remote Sensing Environment* 50:1-17. https://doi.org/10.1016/0034-4257(94)90090-6

Denger, t., Looms, M.C., Sonnenborg, T.O., Jensen, K.H. (2020). Comparison of evapotranspiration estimates using the water balance and the eddy covariance methods. *Vadose Zone Journal,* 19(1). https://doi.org/10.1002/vzj2.20032

Douglas, J.H., Pinter Jr., P.J., Kimball, B.A. (2005). Wheat basal crop coefficients determined by normalized difference vegetation index. *Irrigation Science,* 24, 1–14. doi: 10.1007/s00271-005-0001-0

Duncan, E.W., Kleinman, P.J.A., Folmar, G.J., Saporito, L.S., Feyereisen, G.W., Budan, A.R., Vitko, L., Collick, A., Drohan, P., Lin, H., Bryant, R.B., Beegle, D.B. (2017). Development of Field-Scale Lysimeters to Assess Management Impacts on Runoff. *Transactions of the ASABE,* 60(2), 419-429. doi: 10.13031/trans.11901

Evett, S.R., Marek, G.W., Colaizzi, P.D., Copeland, K.S., Ruthardt, B.B. (2022). Methods for downhole soil water sensor calibration-Complications of bulk density and water content variations. *Vadose Zone Journal.* doi: 10.1002/vzj2.20235

Evett, S.R., Schwartz, R.C., Tolk, J.A., Howell, T.A. (2009). Soil Water Profile Content Determination: Spatiotemporal Variability of Electromagnetic and Neutron Probe Sensors in Access Tubes. *Vadose Zone Journal,* 8(4), 926-941. doi: 10.2136/vzj2008.0146

ESRI, 2011. ArcGIS Pro Desktop: release 10. Redlands, CA: Environmental Systems Research Institute.

Gao, r., (2023). Assessment of Evapotranspiration, Transpiration, and Water Stress Using sUAS Information Over Commercial Vineyards Across Central California. [Doctoral dissertation, Utah State University].

Gunzinski R., Nieto, H., Sánchez, R. R., Sánchez, J. M., Jomaa, I., Zitouna-Chebbi, R., Roupsard, O., López-Urrea, R. (2023). Improving field-scale crop actual evapotranspiration monitoring with Sentinel-3, Sentinel-2, and Landsat data fusion. *International Journal of Applied Earth Observation and Geoinformation,* 125. https://doi.org/10.1016/j.jag.2023.103587

Irmak, Ss., Payero, O.J., VanDeWalle, B., Rees, J., Zoubek, G. (2014). Principles and Operational Characteristics of Watermark Granular Matrix Sensor to Measure Soil Water Status and Its Practical Applications for Irrigation Management in Various Soil Textures. *Biological Systems Engineering: Papers and Publications,* 332.

Katimbo, A., Rudnick, D.R., DeJonge, K.C., Lo, T.H., Qiao, X., Franz, T.E., Nakabuye, H.H., Duan, J (2022a). Crop water stress index computation approaches and their

sensitivity to soil water dynamics. *Agricultural Water Management*, 266. https://doi.org/10.1016/j.agwat.2022.107575

Katimbo, A., Rudnick, D.R., Liang, W., DeJonge, K.C., Lo, T.H., Franz, T.E., Ge, Y., Qiao, X., Kabenge, I., Nakabuye, H.N., Duan, J. (2022b). Two source energy balance maize evapotranspiration estimates using close-canopy mobile infrared sensors and upscaling methods under variable water stress conditions. *Agriculture Water management*, 274. doi: 10.1016/j.agwat.2022.107972

Kustas, W.P., Alfieri, J.G., Anderson, M.C., Colaizzi P.D., Pruegar, J.H., Evett, S.R., Neale, C.M.U., French, A.N., Hipps, L.E., Chávez, J.L., Copeland, K.S., Howell, T.A. (2012). Evaluating the two-source energy balance model using local thermal and surface flux observations in a strongly advective irrigated agricultural area. *Advances in Water Resources*, 50, 120-133, doi: 10.1016/j.advwatres.2012.07.005

Kustas, W.P., Norman, J.M. (1999). Evaluation of soil and vegetation heat flux predictions using a simple two-source model with radiometric temperatures for partial canopy cover. *Agriculture and Forest Meteorology*, 94, 13-29.

Li, F., Kustas, W.P., Prueger J.H., Neale, C.M.U., Jackson, T.J. (2005). Utility of Remote Sensing-Based Two-Source Energy Balance Model under Low-and High-Vegetation Cover Conditions. *Journal of hydrometeorology,* 6(6), 878-891, DOI: https://doi.org/10.1175/JHM464.1

Liang, W., Possignolo, I., Qiao, X., DeJonge, K., Irmak, S., Heeren, D., Rudnick, D. (2021). Utilizing digital image processing and two-source energy balance model for the estimation of evapotranspiration of dry edible beans in western Nebraska. *Irrigation Science*, 39, 617–631. https://doi.org/10.1007/s00271-021-00721-7

Marek, G.W., Evett, S., Marek, T.H., Porter, D.O., Schwartz, R.C. (2023). Field Evaluation of Conventional and Downhole TDR Soil Water Sensors for Irrigation Scheduling in a Clay Loam Soil. *Applied Engineering in Agriculture,* 39(5), 495-507. doi: 10.13031/aea.15574

Mohammed, A. T., Irmak, S. (2022). Maize response to irrigation and nitrogen under central pivot, subsurface drip and furrow irrigation: Water productivity, basal evapotranspiration and yield response factors. *Agriculture Water Management*, 271. https://doi.org/10.1016/j.agwat.2022.107795

Montanaro, M., McCorlkel, J., Tveekrem, J., Stauder, J., Mentzell, E., Lunsford, A., Hair, J., Reuter, D. (2022). Landsat 9 Thermal Infrared Sensor 2 (TIRS-2) Stray Light Mitigation and Assessment. *IEEE Transactions on Geoscience and Remote Sensing*, 60. doi: 10.1109/TGRS.2022.3177312

Nieto, H., Kustas, W.P., Torres-Rua, A., Alfieri, J.G., Gao, F., Anderson, M.C., White, W.A., Song, L., Alsina, M.M., Prueger, J.H., McKee, M., Elarab, M., McKee, L.G. (2018). Evaluation of the TSEB Turbulent Fluxes using different methods for the retrieval of soil and canopy component temperatures from UAV thermal and multispectral Imagery. Irrigation Science, 37, 389-406. https://doi.org/10.1007/s00271-018-0585-9

Norman, J.M., Kustas, W.P., Humes, K.S. (1995). Source approach for estimating soil and vegetation energy fluxes in observations of directional radiometric surface temperature. *Agricultural and Forest Meteorology,* 77(3–4), 263-293. https://doi.org/10.1016/0168-1923(95)02265-Y.Simić, D., Pejić, B., Bekavac, G., Mačkić, K., Vojnov, B., Bajić, I., Sikora, V. (2023). Effect of Different ET-Based

Irrigation Scheduling on Grain Yield and Water Use Efficiency of Drip Irrigated Maize. *Agriculture,* 13. https://doi.org/10.3390/ agriculture13101994

Singh, R.K., Irmak, A., Irmak, S., Martin, D.L. (2008). Application of SEBAL Model for Mapping Evapotranspiration and Estimating Surface Energy Fluxes in South-Central Nebraska. *Journal of Irrigation and Drainage Engineering*, 134(3), 273-285. doi: 10.1061/(ASCE)0733-9437(2008)134:3(273)

Spaans, E.J.A., Baker, J.M. (1992). Calibration of Watermark soil moisture sensors for soil matric potential and temperature. *Soil Science Department*, 143, 213-217. doi: 10.1007/BF00007875

Steven, M.D. (1993). Satellite remote sensing for agriculture management: opportunities and logistic constraints. *ISPRS Journal of Photogrammetry and Remote Sensing*, 48(4), 29–34. https://www.sciencedirect.com/science/article/pii/092427169390029M

Song, L., Kustas, W.P., Liu, S., Colaizzi, P.D., Nieto, H., Xu, Z., Ma, Y.,Li, M., Xu, T., Agam, N., Tolk, J.A., Evett, S.R. (2016). Applications of a thermal-based two-source energy balance model using Priestley-Taylor approach for surface temperature partitioning under advective conditions. Journal of Hydrology, 540, 574-587. 10.1016/j.jhydrol.2016.06.034

Sun, H., Kopp, K., Kjelgren, R. (2012). Water-efficient Urban Landscapes: Integrating Different Water Use Categorizations and Plant Types. *HortScience,* 47(2), 254-263. doi: 10.21273/HORTSCI.47.2.254

Trout, T., DeJonge, K.C. (2018). Crop Water Use and Crop Coefficients of Maize in the Great Plains. *Journal of Irrigation Drainage Engineering,* 144(6). doi: 10.1061/(ASCE)IR.1943-4774.0001309.

Tunica, E. (2023). Evaluating the performance of the TSEB model for sorghum evapotranspiration estimation using time series UAV imagery. *Irrigation Science*. https://doi.org/10.1007/s00271-023-00887-2

Umargono, E., Suseno, J.E., Gunawna, V.S.K. (2019). K-Means Clustering Optimization using the Elbow Method and Early Centroid Determination Based-on Mean and Median. *Proceedings of the International Conferences on Information System and Technology,* 234-240. DOI: 10.5220/0009908402340240

Valentín, F., Sánchez, J.M., Martínez-Moreno, A., Intrigliolo, D.S., Buesa, I., López-Urrea, R. (2023). Using on-the-ground Surface Energy Balance to Monitor Vine Water Status and Evapotranspiration Under Deficit Irrigation and Rainfed Conditions. *Agricultural Water Management,* 281. https://doi.org/10.1016/j.agwat.2023.108240

Appendix

Figure 26

Station 1 2022 FoC Timeseries

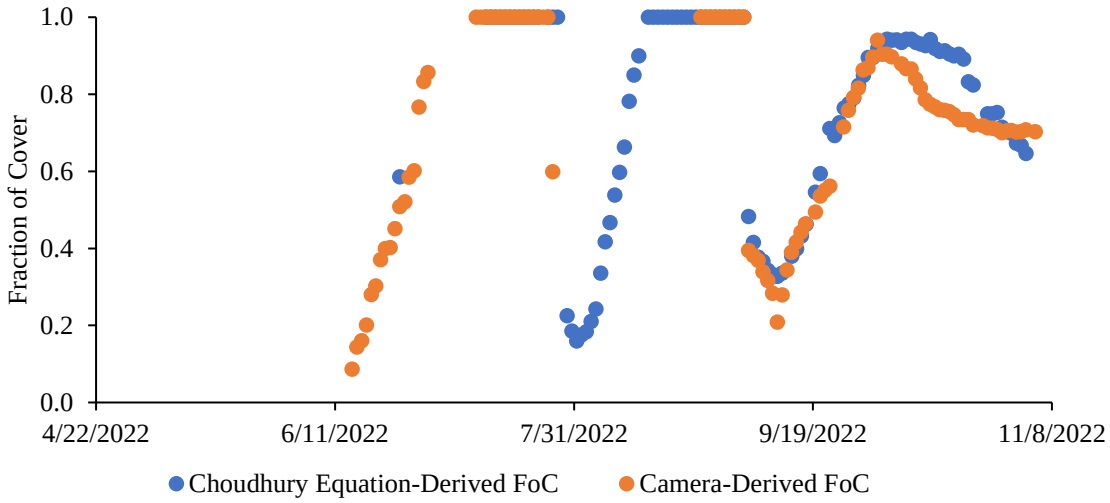

Figure 27

Station 2 2022 FoC Timeseries

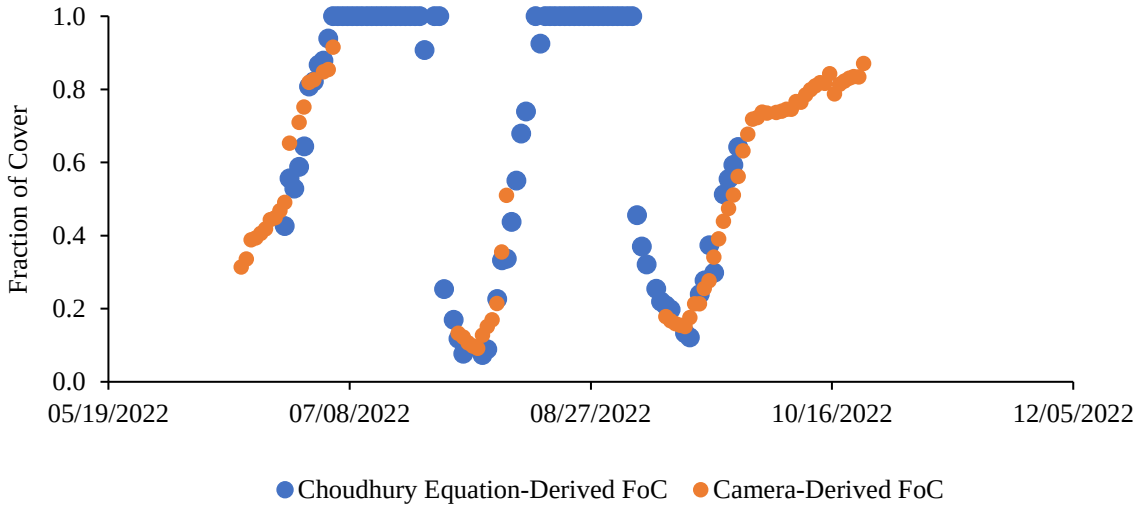

Figure 28

Station 1 2023 FoC Timeseries

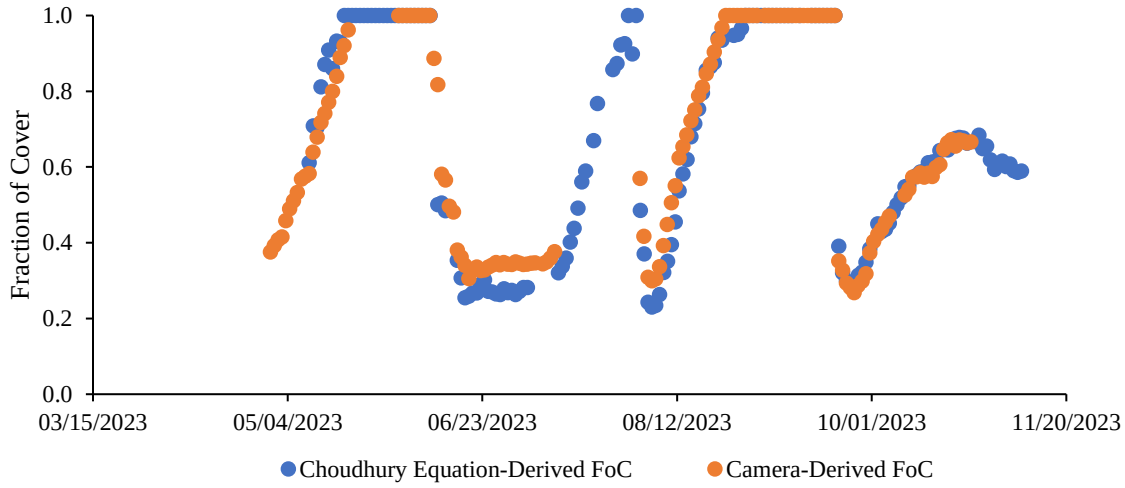

Figure 29

Station 2 2023 FoC Timeseries

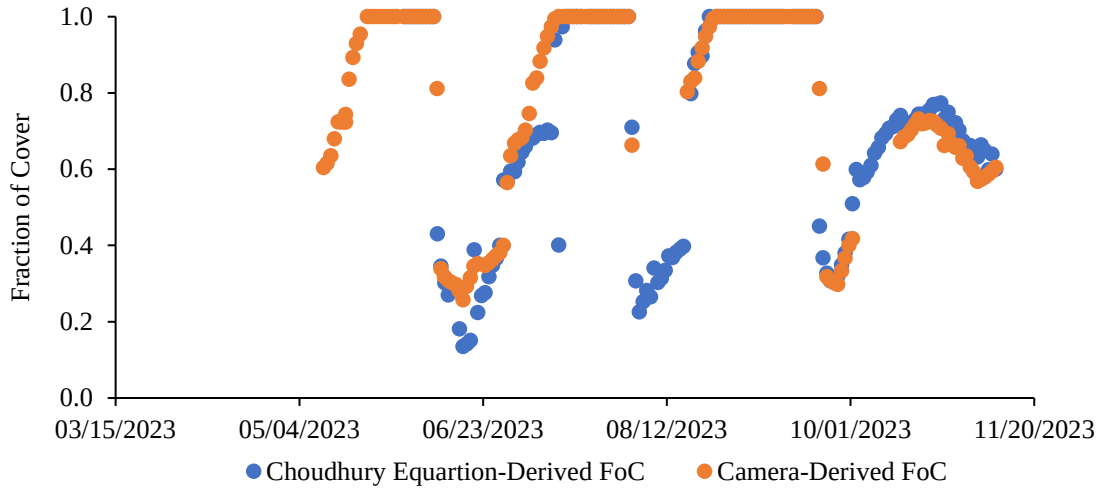

Figure 30

Hourly daytime RSO and Incoming Shortwave

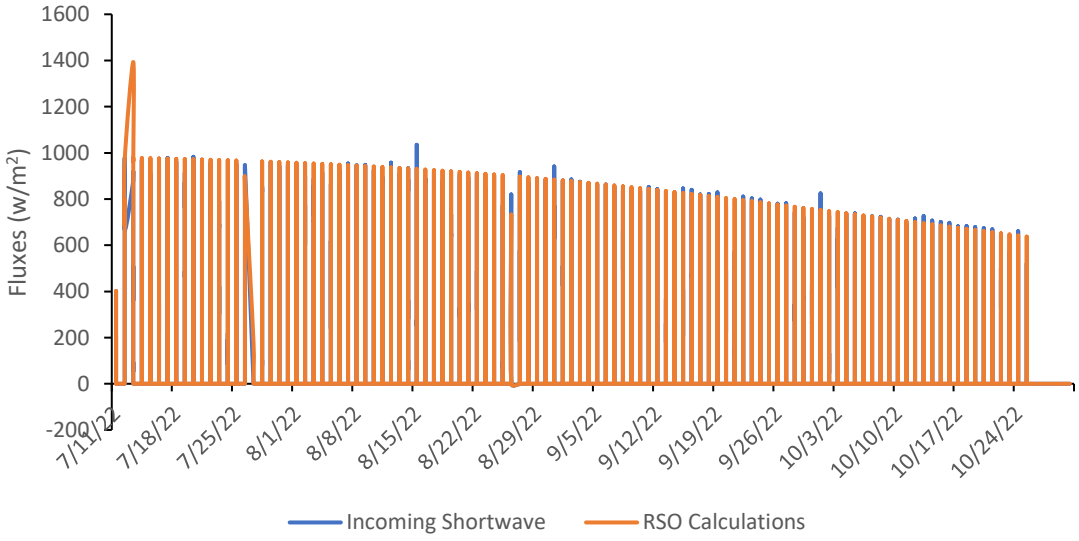

Fig. 31. Hourly daytime RSO and incoming shortwave.

Figure 32

Hourly LE Fluxes with Eddy Covariance G

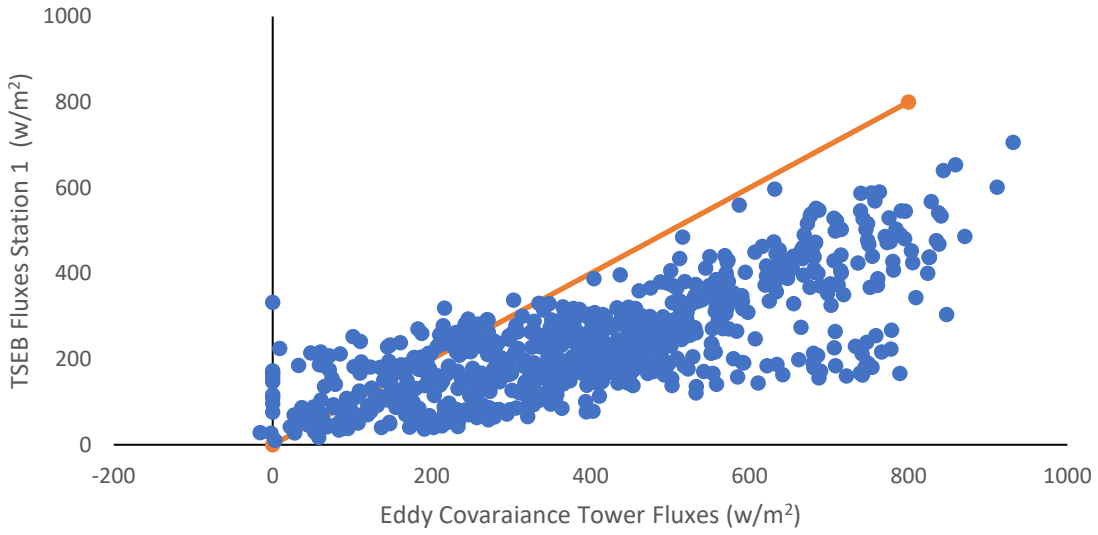

Figure 33

2022 Air Temperature Unity

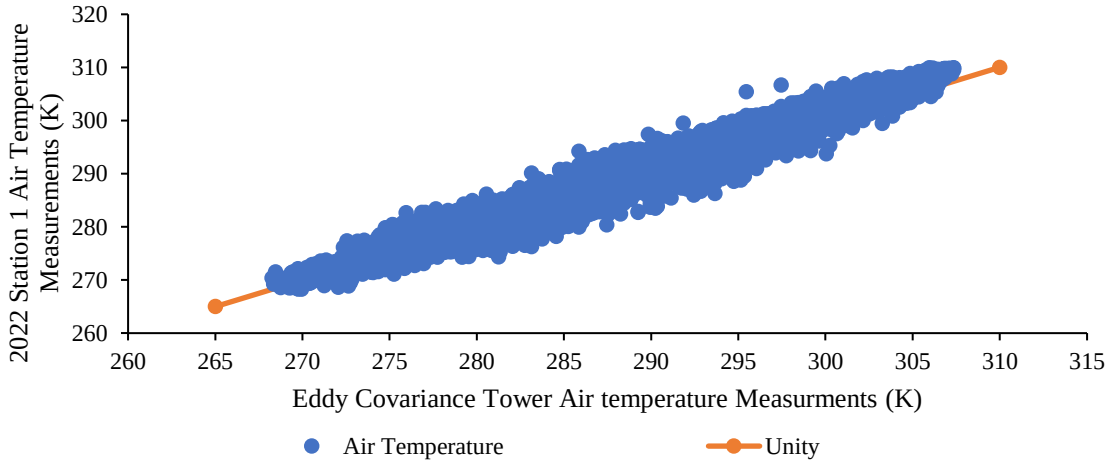

Fig. 34. 2022 air temperature unity.

Figure 35

2022 Vapor Pressure Unity